Commodity Prices Co-movements and Financial Stability: a Multidimensional Visibility Nexus with Climate Conditions

Andrea Flori* Fabio Pammolli†‡ Alessandro Spelta §

Abstract

This paper investigates the nexus between climate-related variables, commodity price co-movements and financial stability. First, we project the commodity price time series onto a multilayer network. Centrality measures computed on the network are used to detect the existence of common trends between the series and to characterize the role of different nodes during phases of market downturns and upturns, unveiling the onset of financial instability. Then, an econometric analysis is introduced to show how climate-related variables affect financial stability by influencing co-movements of commodity prices. Overall, the paper reveals how synthetic indicators of commodity price co-movements generate valuable signals to study the nexus between climate-related conditions and the dynamics of financial systems.

keywords: Commodity Prices; Co-movements; Multilayer Networks; Climate Change; Financial Stability
JEL: C1; G0; G1

*Impact, Politecnico di Milano, Department of Management, Economics and Industrial Engineering; andrea.flori@polimi.it

†Impact, Politecnico di Milano, Department of Management, Economics and Industrial Engineering; fabio.pammolli@polimi.it

‡Center for Analysis, Decisions, and Society (CADS) - Human Technopole and Politecnico di Milano, Milano, Italy

§University of Pavia, Department of Economics and Management, Pavia, Italy

1 Introduction

Governor Carney pointed out that "*Climate change is the Tragedy of the Horizon*", in his speech to the Lloyd's of London in 2015 (Carney, 2015). Notwithstanding the increasing attention by scholars and policy-makers on climate change risks for the economy and society at large, still there is a heated debate on how to properly evaluate externalities and design appropriate policies (see Nordhaus, 1994; McKibbin and Wilcoxen, 2002; Stern, 2008; Nordhaus, 2007). Many economic activities from international trade (Mattoo et al., 2009; Brack, 2013) to agriculture (Howden et al., 2007; Nelson et al., 2009), consumer behavior (Whitmarsh, 2009; Wells et al., 2011) and even tourism (Hamilton et al., 2005; Becken and Hay, 2007) are, in fact, not immune from exposures to climate change. Globalization processes are also likely to favor such economic vulnerabilities (see o'Brien et al., 2004; Leichenko et al., 2010). No less important, the interlinkages between economic activities and changes in the environmental-related systems have been also influenced by the rapid rate of variation of climate conditions, whose dynamics and projections still have to be fully explored (see Houghton et al., 1991; Alley et al., 2003; Meehl et al., 2007; Collins et al., 2013).

The financial industry has started to exploit these sources of instability by proposing devoted financial products for investment or hedging purposes. This is the case, for instance, of insurance policies against specific natural risks or catastrophic single/multi events (e.g., flooding, droughts, earthquakes, hurricanes, wildfires, etc.), or the issuance of catastrophic bonds (CAT bonds) to share certain risks with capital markets. The exploitation of instability sources has also stimulated pre- and post-disaster financial arrangements to foster risk mitigation and finance the recovery. More recently, the Conference of Parties (COP), held in Paris in 2015, posed clear commitments to ensure that financial markets play a full and constructive role to address climate change by facilitating, for instance, clean investments, the pooling of climate-related risks, and the adoption of appropriate stress testing procedures to enhance financial stability during the transition to a low-carbon economy (see Farid et al., 2016).

Indeed, financial markets have been recognized as increasingly responsive to climate change. More in general, the transmission mechanisms of risks from climate change to financial systems and individual institutions envision a multidisciplinary research agenda (see, e.g. Stolbova et al., 2018). Dietz et al. (2016), for instance, estimate the "climate value at risk" of global financial assets when carbon emissions are cut to limit warming to no more than 2^oC, while Dafermos et al. (2018) find that climate change can impact on financial stability by deteriorating firm liquidity and by reducing the price of corporate bonds and the supply of credit. Moreover, Battiston, Mandel, et al. (2017) extend the concept of climate value at risk to individual institutions through network analysis and propose a stress-test procedure taking into account financial dependencies to evaluate the degree to which financial institutions are exposed to sources of climate risk. The authors study portfolio composition in terms of green (or brown) investments and find that investors' equity holdings bear large exposures to climate-policy-relevant sectors and that a late climate policy adoption could have adverse systemic consequences.

Climate change can, in fact, influence the stability of financial systems directly through more frequent and severe disasters impacting the economy, while the uncertainty related to the re-conversion process into a low-carbon economy and its timing and speed can potentially determine disruptive variations on the asset prices of carbon-intensive sectors and pose major risks and opportunities to society at large (Giuzio et al., 2019). Therefore, the assessment of stability conditions of capital markets should also take into account the complex and evolving exposures due to the risks associated to climate change and environmentally-related phenomena. Financial systems are thus not immune from these risks and a proper evaluation of the interdependencies between climate change and financial stability call for novel approaches and indicators able to monitor and assess how environmental and climate-related risks might propagate throughout the financial systems and wider economy (see Battiston, Mandel, et al., 2017). For instance, Pollitt and Mercure (2018) discuss the role of the financial sector in the assessment of macroeconomic costs and benefits induced by climate and energy policies, while Stolbova et al. (2018) propose a network-based approach to trace feedback loops between the financial sector and the real economy and to assess how climate policy-induced shocks impact on virtuous or vicious cycles that arise in the climate-finance nexus.

Against this background, commodity markets represent a relevant domain to study the nexus between financial systems and environmental and climate-related dimensions. In fact, commodities, besides being traded for speculative purposes, are exchanged because of their underlying role for nutrition needs or as inputs for production activities. Since the production of commodities is also affected by environmental factors, climate change may have a substantial impact on their prices and, ultimately, on the financial stability of the corresponding markets. Literature has already recognized the critical implications of climate change on agricultural commodities, in terms of production, availability and security (see Fischer et al., 1994; Parry et al., 1999; Brown and Funk, 2008; Wheeler and Von Braun, 2013; Springmann et al., 2017). In addition, these spillover effects appear mutually reinforced. For instance, greenhouse gas emissions from food-related activities limit the reduction of global warming, while increasing temperatures and declining precipitation depress the production of corn, wheat, rice, and other primary crops. Even worse, at local levels, small farmers of food-insecure regions often rely on their own production to meet their food needs and are, therefore, more exposed to sudden climate variations and extreme natural events. These drops in agricultural production can therefore influence the national fiscal balances of poorly developed countries that heavily depend on the agricultural sector, thus limiting their role in trade systems and, ultimately, their ability to meet domestic food needs through the capacity of import from other markets. Furthermore, globalization and interconnected financial markets contribute to the spread of the externalities from climate change and influence commodity prices globally. Hence, climate change could potentially slow down the efforts made for a world without hunger and reverse the converging trajectories for those regions that are more dependent on the agricultural production. By affecting both external and domestic imbalances, variations in commodity prices may have substantial effects on the stability of these economies.

Several empirical studies investigate co-movements between climate change and commodities, specifically among those related to food and agricultural materials. For instance, Hong et al. (2019) note that food stock prices underreact to climate change risks, while Piot-Lepetit and M'Barek (2011) argue that price volatility of agricultural commodities cannot be analyzed as financial price volatility. Interestingly, a stream of literature focuses on the relationships between agricultural commodities and fuels, thus motivating the selection in our analysis of a wide set of commodities. For instance, Reboredo (2012) observes weak oil-food dependence and no extreme market dependence between oil and food prices. Lucotte (2016) finds strong positive co-movements between crude oil and food prices in the aftermath of the commodity boom that occurred in the last decade, and Baumeister and Kilian (2014) notice that co-movements between the prices of oil and agricultural products appear largely driven by common macroeconomic determinants. Interestingly, complex systems techniques have begun to spread in these contexts to study co-movements across various types of environmental-related time series. For instance, Filip et al. (2016) propose a combination of minimum spanning trees correlation filtration and wavelet analysis to analyze the interconnections between biofuels and financial factors, while Kristoufek et al. (2012) apply a minimum spanning tree analysis on a similar sample and find that the average tree lengths suggest that ethanol and biodiesel are very weakly connected with other commodities in the short-term, and that in the medium-term the biofuels network becomes more structured and characterized by a group of fuels and another one of food commodities, and that after the global financial crisis of mid-2007 connections became much stronger.

In this work we investigate how climate-related variables can affect the stability of financial systems by impacting on commodity prices. To this aim, we develop a few synthetic indicators of co-movements among commodity time series that account for both the cross-section and temporal dimension of the series during either upward or downward phases, which we then relate to the study of the nexus with financial stability. Our aim is to provide a set of indicators that could be used to map the stability conditions of financial systems in line with a common perspective in the literature on systemic risk and financial stability that addresses other similar sources of risks combining both a micro and a system-wide perspective to extract signals of the transition in the behavior of the underlying system from directional and coordinated market patterns. Hence, we opt for a parsimonious representation of directional co-movements to map market dynamics that may lead to phases of instability, thus providing synthetic indicators useful for scrutinizing and monitoring market stability in a timely manner, consistently with other proposed indicators and perspectives entered in the risk dashboard for systemic risk in wider capital markets.

In so doing, we first explore the temporal properties of individual commodity time series. Financial asset series, besides being typically non-stationary, are likely to present nonlinear structures, which may mask the presence of long-range temporal dependence, or time reversibility, i.e., the degree of dynamic invariance under time reversal (see Flanagan and Lacasa, 2016; Roldán and Parrondo, 2010; Roldán and Parrondo, 2012). Recently, several approaches have been proposed to convert time series into graphs that encode some features of the original time series into nodes and edges without assuming any specific functional form for the data generating processes. In particular, visibility graph methods have been shown to overcome some time series analysis limitations, especially when dealing with complex phenomena (see Lacasa et al., 2009; Lacasa et al., 2012; Lacasa et al., 2015).

In fact, visibility methods create graphs which inherit relevant features of the original time series in both stationary and non-stationary systems (Lacasa and Flanagan, 2015). In particular, the method proposed in Lacasa et al. (2008) and Lacasa et al. (2009), namely the *Natural Visibility Graph*, transforms a time series into a graph according to a mapping algorithm linking points of the time series according to a convexity criterion. In the resulting graph, every node corresponds to a time-stamp data point and two nodes are connected if they are visible from each other, i.e., if there exists a straight line connecting them and not intersecting the height of any other intermediate time-stamps. Compared to other methods employed to transform times series into networks (see Xu et al., 2008; Strozzi et al., 2009; Donner, Small, et al., 2011), visibility graph algorithms have a straight-forward geometric interpretation of the original time series, thus making them suitable for quantitative analysis of financial market series.

Specifically, by applying the visibility criterion of Lacasa et al. (2008), a periodic series is transformed into a regular graph, a random series into a random graph, while a fractal series is converted into a scale-free graph. Since the visibility graph of a fractal time series follows a power law degree distribution, the self-affine characteristic of a time series can be analyzed by means of the power-law exponent of the degree distribution of the associated graph rather than being investigated by means of statistical techniques like the Hurst exponent. Here, we employ this graph-embedded approach to study how phenomena, such as long-range dependence, may lead to phases of market instability.

To discriminate between market upturns and downturns, we introduce a novel configuration of the visibility graph that results in a directed network, namely the *Direct Visibility Algorithm*. The Direct Visibility Algorithm produces a directed network for each commodity time series where the minima (maxima) of the time series are mapped into nodes with high values of the out- (in-) degree according to a predefined ordering criterion. Then, to characterize commonalities across multiple commodity prices time series, we introduce a probabilistic tensor decomposition (see Kolda et al., 2005; Avdjiev et al., 2019), which we apply on top of the visibility graph. In a nutshell, the probabilistic tensor decomposition produces centrality indicators, i.e. Hub and Authority scores[1], for each time observation using the information embedded in the multilayer visibility network. Similarly to the in-(out-)degree, which reveals local maxima (minima) of a single time series, the Authority (Hub) score provides information on coordinated maxima (minima) in a multivariate setting, such that the higher the Authority (Hub) score associated to a certain node, the more the corresponding commodity time series show a coordinated behavior on positive (negative) trends. Additionally, Authority and Hub scores are characterized by a self-reinforcement mechanism, being feedback centralities. Authority scores are, in fact, higher for time stamps with significant links from nodes with high values of the Hub score, and similarly Hub values are higher for those nodes with significant connections to high-valued Authority time points. Thus, central nodes of the multilayer visibility network do not simply identify aligned maxima or minima on multiple series, but they also convey information on the return time distribution of the series, where the return time is defined as the shortest time required by the system to visit the same state from which it started to move (see Ding and Yang, 1995). This information is important, since it helps detecting the emergence of abrupt transitions between different market phases.

Although time series analysis is a mature and solid field with well developed and understood methods and associated theory, this type of analysis still has some limitations when it is applied to the study of more complex signals, e.g. when time series are non-linear or exhibit long-range memory, chaotic behaviors and intermittency. Our proposed approach is instead parameter free and does not require any assumption on the functional form of the data generating process. In particular, the study of nodes centrality allows us to investigate some relevant non linear properties of the multilayer network, such as system synchronization. Indeed, the presence of central nodes reveals an increased synchronisation of commodity prices, which occurs when the system is driven away from its equilibrium configuration. Conversely, nodes centrality results more evenly distributed during periods of market stability, when the system is close to equilibrium (see Lacasa et al., 2015). In other words, multilayer centrality scores uncover the emergence of synchronized patterns between commodity prices and can be used to measure the intensity of self-organizing processes arising from market co-movements and positive feedbacks (see Heemeijer et al., 2009; Flori et al., 2019; Spelta et al., 2020).

Finally, we employ Granger causal connectivity analysis (Granger, 1969) for assessing the directional functional connectivity between climate-related series (namely, temperature, air pressure, rainfall and wind directions), our proposed topological centrality scores and the FED Financial Stress Index (FSI), which is employed as a proxy for financial stability[2]. Our results reveal a synchronization between extreme values of the centrality

[1]The words centrality, score and ranking are used as synonymous in this paper.

[2]St. Louis Fed Financial Stress Index, retrieved from FRED, Federal Reserve Bank of St. Louis; https://fred.stlouisfed.org/series/STLFSI, February 21, 2019.

measures and those of the climate-related variables. We also show the presence of a lead-lag effect between the FSI and the topological measures, highlighting a nexus between commodity price co-movements and capital markets. These findings are also supported by the application of the Toda and Yamamoto's variant of the Granger causality test (see Toda and Yamamoto, 1995) and by the impulse-response analysis estimated by local projections (Jordà, 2005). From a macro-prudential perspective, our analysis thus aims to contribute to the debate on explainable forecasting approaches about the transmission mechanisms behind the interlinkages between climate, macroeconomics and financial systems.

Our work is also coherent with the recent perspective on disaster risk management provided in the Global Assessment Report on Disaster Risk Reduction (2019) of the UN Office for Disaster Risk Reduction (UNDRR), which explicitly refers to the presence of increasingly complex interactions among hazards and human relationships that should be addressed, monitored and mitigated using a complex systemic risk assessment (UNDRR, 2019). The study of financial instability and the role played by natural risks and climate-related conditions in shaping market reactions urge, therefore, a new set of techniques and methodologies able to monitor in almost real-time the stability conditions of financial systems against natural shocks and climate-related threats.

The paper is organized as follows. In Section 2 we discuss the data set used in the analysis. We then introduce the methodology employed to convert the commodity price time series into visibility graphs and we present the tensor decomposition, which we use to synthesize, through centrality measures, the importance of each period in terms of co-movements among commodity time series. Section 3 reports the results of the study and the econometric investigation concerning the relationships among the co-movement indicators, climate-related variables and financial stability. Section 4 concludes our study and discusses some limitations of our analysis.

2 Data and Methodology

2.1 Data

Our analysis considers relationships among three different layers of analysis referring to the environmental, financial and commodity dimensions, the latter that links the first two. The three dimensions are represented by various types of data: i) price times series for a broad range of commodities, ii) environmental-related variables, and iii) an aggregate financial index for overall stability conditions in capital markets. As regards the first set of variables, we employ monthly price time series of 42 commodities along the period from January 1980 to June 2017. Data are retrieved from FRED and are expressed in USD. These series are intended to cover a wide spectrum of commodity markets in order to explicitly verify the extent of co-movements in different economic contexts. Specifically, the series can be referred to the following broad categories[3]:

- Agriculture and Food: Bananas, Barley, Beef, Cocoa, Coffe Arabica, Coffe Robustas, Corn, Fish, Fish Meal, Groundnuts, Lamb, Olive Oil, Oranges, Palm Oil, Poultry, Rapeseed Oil, Rice, Shrimp, Soybeans Oil, Soybeans, Sugar, Sunflower Oil, Swine, Tea, Wheat;

- Fuels and Oil: Brent Crude, Dubai Crude, WTI Crude, Coal;

[3]Some series have specific geographical connections, which is the case, for instance, of: Coal (Australia), Oil (Europe, Dubai), Rice (Thailand) or Tea (Kenya).

- Metals: Aluminium, Copper, Iron Ore, Lead, Nickel, Tin, Zinc;
- Other: Cotton, Hides, Rubber, Soft Logs, Wool Coarse, Wool Fine.

As environmental variables, we include monthly data on rainfall, temperature, atmospheric pressure and wind strength, which although far from providing a granular representation of climate and environmental phenomena still provide a reasonable framework for relevant dimensions that may impact on the selected list of commodities. In particular, average rainfall rate values refer to five satellite estimates (namely, GPI, OPI, SSM/I scattering, SSM/I emission and MSU). As temperature we consider global land surface temperatures from the Global Historical Climatology Network and the Climate Anomaly Monitoring System (GHCN + CAMS). From NCEP/NCAR Reanalysis we retrieve the atmospheric pressure at the sea level and the direction and strength of the wind (for detailed information on climate series, see Xie and Arkin, 1997; Jones, Osborn, et al., 2001; Brohan et al., 2006; Fan and Van den Dool, 2008; Jones, Lister, et al., 2012). For each climate variable, we use a grid of monthly observations formed by latitude and longitude coordinates. For the scope of the paper, we construct proxies for the related dimension by averaging across the grid points the time records. Finally, since climate processes can be influenced by seasonal factors, we apply curve fitting on sine/cosine waves to purge data from cyclical components[4]. This procedure allows us to extract the global trends of the time series, free from the effect of known seasonality with fixed and known periodicity. Thus, by removing a nuisance periodic component we produce de-seasonalized time series useful for exploring the trend and any remaining irregular component.

We address the overall financial stability conditions by comparing our topological indicators with the FED Financial Stress Index (FSI), which measures the degree of financial stress in capital markets. The indicator combines seven interest rate series, six yield spreads and five other indicators (e.g., for bonds issued in emerging markets, for inflation dynamics or market volatility such as the VIX indicator), without directly including commodity price series. Overall, FSI is intended to provide a comprehensive picture of stability conditions across multiple financial systems. Accordingly, when the level of financial stress in the markets varies, these data series are likely to co-move. In practice, values of the indicator below zero indicate below-average financial stress, while values above zero stand for above-average financial market stress (Kliesen, Smith, et al., 2010; Kliesen, Owyang, et al., 2012).

Figure 1 shows the behavior of the de-seasonalized climate series along with the Financial Stress Index. Average rainfall, for instance, exhibits a sharp increase after 2011, while the average temperature shows a growing pattern in the last decades; by contrast, the average pressure and wind directions are almost stable in the sample period, although the latter show a few remarkable variations at the end of the sample period. Overall, these series seem to point to changes in environmental conditions especially in the last period. Finally, we report the time series for the FSI that peaks during the global financial crisis of mid-2007, while it indicates below-average financial stress for more recent observations in the sample.

[4]We have applied a seasonal filter to deseasonalize time series using a multiplicative decomposition, meaning that before estimating the seasonal component we have removed the linear trend applying a 12-term symmetric moving average. This allows us to divide the original series by the smoothed series to detrend the data. Then, we have employed a seasonal curve fitting on sine/cosine waves to the desesonalize series.

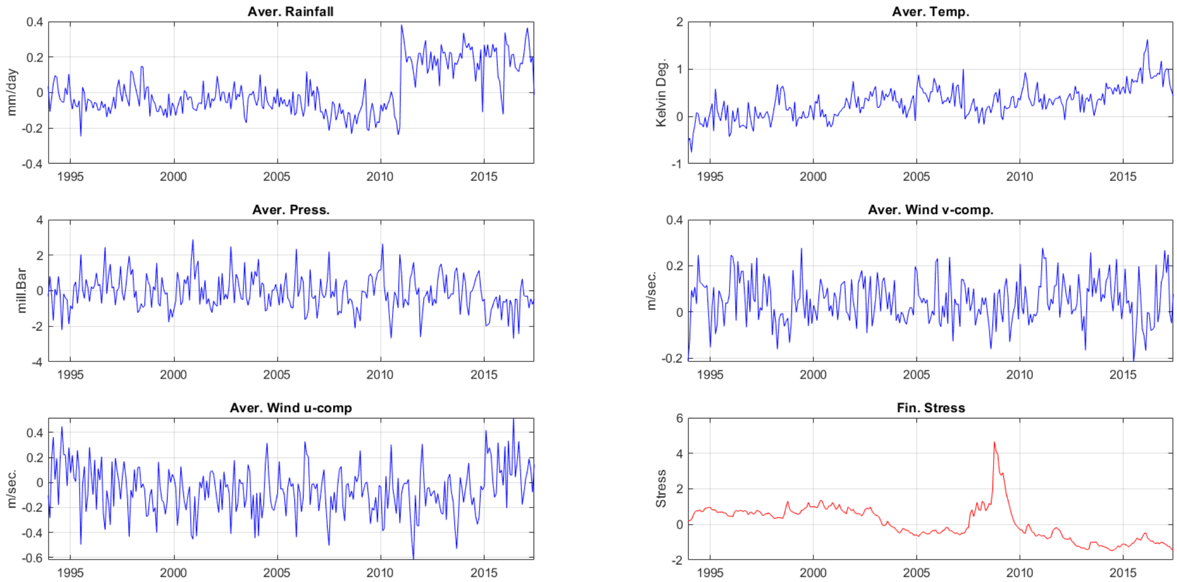

Figure 1: De-seasonalized climate series and the Financial Stress Index. The figure shows the temporal patterns of the climate-related time series after removing the seasonality components (blue lines), together with the FSI of the Federal Reserve Bank of St. Louis (red line).

2.2 Directed Visibility Graph

Graph-theoretical tools are key solutions to convey general information on the dynamics of a system when its precise mathematical description is not possible (see Pammolli and Riccaboni, 2002; Spelta et al., 2019). The analysis of a system by means of a graph-theoretical approach at different time points can be exploited to detect regime shifts (see Orsenigo et al., 2001). In other words, these graph-theoretical techniques can be applied to extract relevant information about the evolution of a system in a simple and parsimonious way (see also Lacasa et al., 2008; Xu et al., 2008; Strozzi et al., 2009; Donner, Small, et al., 2011).

From a risk assessment perspective, we propose and test a few synthetic indicators able to map how co-movements among commodity time series can signal market instability. In so doing, the use of visibility graph has to be seen as instrumental for constructing adjacency matrices which are then used to build the tensor and extract centrality scores from its decomposition as proxies for co-movements toward market trends. In order to do so, visibility graph algorithms are considered as the bridge between time series and the complex system literature, in which the values assumed by a time series are plotted as vertical bars, and two bars (time stamps) are connected if they can "see" each other. Importantly, the structure of time series conserves when it is converted to graph (see Lacasa et al., 2008; Lacasa et al., 2009) and the topological properties of the resulting graph allow to study emerging phenomena, such as the long-range dependence, which are at the ground level of many phases of market instability.

The visibility approach has been shown, in fact, to be a simple, computationally efficient and analytically tractable technique, which can be used to extract relevant information about the original signals of a series. The process generating the time series can be characterized by using a graph theoretical measure that inherits several key structural properties of the original series. In particular, Lacasa et al. (2009) show that nonstationary time series with long-range dependence, such as a fractional Brownian motion, can be depicted as a scale-free visibility graph with degree distribution depending on the Hurst exponent of the series, while in Lacasa et al. (2012) they combine visibility graph with the Kullback-Leibler divergence to both convert a time series into a network based on a geometric criterion and correctly distinguish between reversible and irreversible stationary time series. Moreover, visibility graphs have been shown to be invariant under several transformations of the time series, such as translation, re-scaling and addition of a linear trend to the data (see Lacasa et al., 2008).

Recently, many different methods and applications of visibility graph algorithms have been proposed in many fields, such as economics (see, e.g., Qian et al., 2010; Wang et al., 2012), geology (see, e.g., Donner and Donges, 2012), biology (see, e.g., Ahmadlou et al., 2010; Hou et al., 2016), transportation (see, e.g., Tang et al., 2016). From a technical perspective, several modifications of the traditional visibility graph approach have been proposed so far, such as the horizontal visibility graph (HVG) (Lacasa et al., 2009), and the multi-scale limited penetrable visibility graph (LPVG) (Gao et al., 2016), which mainly focus on different ways of building visibility graphs. In our work, we propose a variant of the Natural Visibility algorithm of Lacasa and coauthors to take into account the direction of the links. This step is instrumental to assess co-movements during either upward or downward phases, which we then relate to the study of the nexus with financial stability. In fact, despite the fact that the Natural Visibility algorithm produces a graph in which the most connected nodes correspond to the extreme events of the series, the topological features of the resulting undirected graph cannot discriminate between extreme and positive w.r.t. extreme and negative events. For this purpose, we have decided to introduce a novel configuration of visibility graph that results in a directed network. Indeed, the *Direct Visibility* variant of the algorithm produces a directed network where the maxima (minima) of the series are mapped into nodes with a high value of the in-(out-)degree according to a predefined ordering criterion.

More specifically, suppose to define an (arbitrary) ordering criterion of the series such that in the resulting graph the links will be directed from the time stamps (nodes) in which the series have lower values to the time stamps that have higher values[5], if and only if there are no intermediate points with higher values between them (as in the Natural Visibility case). Such Direct Visibility variant allows us to map local maxima and minima of commodity prices series into nodes with high values of the in-degrees or out-degrees, respectively. The degree distribution is thus instrumental for discriminating between periods approaching market downturns and upturns.[6] Formally, the following visibility criteria provide a way to draw edges connecting pairs of time stamps, thus forming the backbone structure of the visibility graph. In formulae, two arbitrary time points t_a and t_b with values y_a and y_b are connected with a directed link $A(a,b) = 1$ if, for every other point $t_c \in (t_a, t_b)$, they satisfy:

$$A(a,b) = 1 \quad \text{if} \quad y_a < y_b \quad \text{and} \quad y_c < y_b + (y_a - y_b)\frac{t_b - t_c}{t_b - t_a} \tag{1}$$

Figure 2 shows, through simulations, that the proposed algorithm is effectively able to map those time stamps where the corresponding series present high (low) values into nodes with high in- (out-) degrees. Since asset prices have been shown to display statistical features inherited from power law distribution (see, e.g., Gabaix et al., 2003; Plerou et al., 2004), we generate data from such distribution. We extract series of 1000 values, repeating the experiment 1000 times, and for each repetition we build the adjacency matrix related to formula (1). Then, the in- and out-degree of each node was reported against the height

[5] The ordering criteria is arbitrary and can also be reverted.

[6] In Appendix A, Figure A.1 graphically shows the mapping between the values of a simulated series and the resulting network topology.

of the corresponding point in the series. Figure 2 shows that high values of the simulated series, i.e., maxima, are mapped into nodes with a high in-degree and, conversely, low values of the series, i.e., minima, are mapped into nodes with a high out-degree.

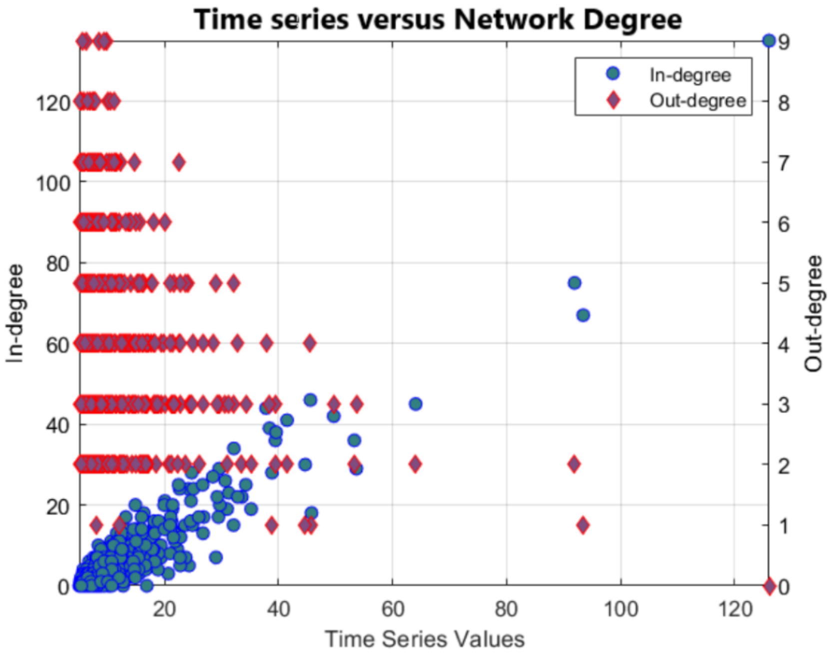

Figure 2: In- and out-degree versus time point height. The figure reports the results of the simulation analysis on the functioning of the Direct Visibility algorithm by showing its ability to map high (low) time point values into nodes with high in-(out) degree values. The figure displays the in- and out-degree of each node against the height of the time point. Time stamps with high values are mapped into nodes with a high in-degree and, conversely, time stamps associated with low values of the series are mapped into nodes with a high out-degree.

Despite their wide applications in different fields, visibility graphs have been almost entirely devoted to the analysis of univariate time series (an exception is Lacasa et al., 2015). In order to cope with this gap, we propose a tensorial approach that produces centrality measures in a multidimensional setting, simultaneously addressing the cross-sectional and the time dimensions of the commodity price time series by jointly considering all the visibility graphs together in a single multidimensional object (see Kolda and Bader, 2009; Avdjiev et al., 2019).

2.3 Probabilistic Tensor Decomposition

In this Section we show how a probabilistic tensor decomposition applied to a visibility multilayer network can be used to extract relevant features about price relationships encoded in the network through centrality measures. In particular, we show that these structural descriptors of the corresponding multilayer network reveal the transition between different dynamical phases and the onset of system synchronization stages.

In our analysis, for each commodity time series k of length T we apply the aforementioned formula (1) to build a directed visibility graph described by an adjacency matrix V_k of size $T \times T$. The resulting matrices are then stacked into a single mathematical object, namely a three-way tensor $\mathcal{V} \in \mathbb{R}^{T \times T \times K}$. Formally, following Kolda and Bader (2009) and Spelta et al. (2018), the 3-rd order tensor is an element of the tensor product of three vector spaces, each of which has its own coordinate system. The multilayer network in which each layer represents the visibility graph associated with a single commodity series can thus be mapped into a 3-rd order tensor $\mathcal{V} \in \mathbb{R}^{T \times T \times K}$, as we have a 2-dimensional visibility graph for each commodity series k, the latter representing the third dimension.

The tensor decomposition of $\mathcal{V}$ produces three scores that represent the Hub and the Authority scores associated to each node, as well as a Type score related to each layer k (Kleinberg, 1999; Kolda et al., 2005; Kolda and Bader, 2009). Specifically, nodes with high Hub scores represent points in time in which commodity prices co-move on a downward trend, while nodes with high values of the Authority score represent time points where commodity prices co-move upwards. The Type score of each layer contains information on the probability that high scoring time stamps are connected in such layer, i.e., it reveals information on whether time points with high Hub and Authority values connect to each other in that particular commodity time series.

The TOPHITS algorithm developed by Kolda et al. (2005), a generalization of the HITS algorithm (see Kleinberg, 1999) for multidimensional arrays, provides a global centrality measure for nodes and layers by producing one score for each dimension of the tensor under analysis. To obtain centrality measures with a probabilistic interpretation, we modify the TOPHITS algorithm in line with Ng et al. (2011). We propose to compute such centrality scores from the transition probabilities of a Markov chain applied to the tensor, whose joint stationary distributions will be the product of Hub, Authority and Type scores. This has the advantage of a better interpretation of the results, as probabilities are normalized by definition (Avdjiev et al., 2019).

For computing centrality measures, the starting point of the construction of the decomposition is the computation of the (bivariate) conditional frequencies $\mathcal{H}$, $\mathcal{A}$ and $\mathcal{R}$ for Hub, Authority and Type scores, respectively. Let $\mathcal{V} \in \mathbb{R}^{T\times T\times K}$ be the 3-rd order tensor obtained by stacking the adjacency matrices of the visibility graphs $\mathbf{V}_k$ for $k = 1, ..., K$. Each element of the tensor v_{ijk} takes value 1 if nodes i and j are connected in the k-th layer and zeros otherwise or, in other words, it assumes value 1 if time point j is visible from time point i in the k-th time series. Conditional frequencies can thus be obtained by normalizing the entries of the tensor $\mathcal{V}$ as follows:

$$\begin{aligned} h_{i|jk} &= \frac{v_{ijk}}{\sum_{i=1}^{T} v_{ijk}} \quad & i = 1, ..., T \\ a_{j|ik} &= \frac{v_{ijk}}{\sum_{j=1}^{T} v_{ijk}} \quad & j = 1, ..., T \\ r_{k|ij} &= \frac{v_{ijk}}{\sum_{k=1}^{K} v_{ijk}} \quad & k = 1, ..., K \end{aligned} \tag{2}$$

being $h_{i|jk}$ the conditional frequency of visiting the i-th node as a Hub, $a_{j|ik}$ the conditional frequency of visiting the j-th node as an Authority, and $r_{k|ij}$ the conditional frequency of using the k-th commodity layer, given that nodes j and i are currently connected.

To account for the so called dead end nodes, when $v_{ijk} = 0$ the values of $h_{i|jk}$ and $a_{j|ik}$ are set to $1/T$, while the value of $r_{k|ij}$ is put to $1/K$.

From the above quantities we can estimate the conditional probabilities as:

$$\begin{aligned} &Pr[X_\eta = i | Y_\eta = j, Z_\eta = k] \\ &Pr[Y_\eta = j | X_\eta = i, Z_\eta = k] \\ &Pr[Z_\eta = k | X_\eta = i, Y_\eta = j] \end{aligned} \tag{3}$$

where X_η, Y_η and Z_η are random variables referring to the probability that a random walker visits any node as a Hub or as an Authority at step η of the Markov chain, using every type of commodity time series. Such conditional frequencies are then employed to derive the stationary marginal probabilities:

$$\begin{aligned} Pr[X_\eta = i] &= \sum_{j=1}^{T} \sum_{k=1}^{K} h_{i|jk} Pr[Y_\eta = j, Z_\eta = k] \\ Pr[Y_\eta = j] &= \sum_{i=1}^{T} \sum_{k=1}^{K} a_{j|ik} Pr[X_\eta = i, Z_\eta = k] \\ Pr[Z_\eta = k] &= \sum_{i=1}^{T} \sum_{j=1}^{T} r_{k|ij} Pr[X_\eta = i, Y_\eta = j] \end{aligned} \tag{4}$$

In other words, for any Hub node i we assign a non-zero probability of jumping to the Authority node j; this probability is inversely proportional to the number of directed edges exiting from node i multiplied by the probability of using layer type k as transition matrix. Similarly, for any Authority node j we assign a non-zero probability of jumping to a Hub node i that is inversely proportional to the number of directed edges pointing to node j times the probability of using layer type k as transition matrix. Instead, for any layer type k we assign a non-zero probability of being utilized as transition matrix; such probability is inversely proportional to the flow between nodes i and j in all the layers multiplied by the probabilities that nodes i and j are connected in layer k as Hub and Authority, respectively.

Finally, limiting distributions of system (4) can be used as Hub, Authority and Type scores, which are then defined as:

$$\begin{array}{l} \omega_i = \lim_{\eta\to\infty} Pr[X_\eta = i] \\ \theta_j = \lim_{\eta\to\infty} Pr[Y_\eta = j] \\ \gamma_k = \lim_{\eta\to\infty} Pr[Z_\eta = k] \end{array} \tag{5}$$

In line with the TOPHITS algorithm, the three scores can be obtained by solving iteratively the following system of equations:

$$\begin{array}{ll} \omega_i = \sum_{j=1}^{T} \sum_{k=1}^{K} h_{i|jk}\theta_j\gamma_k & i = 1, ..., T \\ \theta_j = \sum_{i=1}^{T} \sum_{k=1}^{K} a_{j|ik}\omega_i\gamma_k & j = 1, ..., T \\ \gamma_k = \sum_{i=1}^{T} \sum_{j=1}^{T} r_{k|ij}\omega_i\theta_j & k = 1, ..., K \end{array} \tag{6}$$

until the converge criterion $|\omega^\eta - \omega^{\eta-1}| + |\theta^\eta - \theta^{\eta-1}| + |\gamma^\eta - \gamma^{\eta-1}| < \epsilon$ is met.

In other words, let K denote the total number of commodity price series for which a visibility graph $\mathbf{V}_k$ is computed and let γ_k be the score corresponding to the importance of the k-th series, i.e., the contribution of the k-th series to the importance of the nodes in the visibility tensor. Moreover, let ω_i and θ_j be the scores corresponding to the importance of the i-th and j-th nodes, i.e., the importance of the i-th and j-th time points across multiple series in terms of out-going and in-coming links, respectively. These two scores represent the Hub and Authority importance associated to the time nodes.

The proposed algorithm can be also related to Correspondence Analysis, which is a standard multivariate statistical technique aiming to analyse frequency tables (see Greenacre, 2017; Lebart et al., 1995). In Correspondence Analysis, a table of frequencies represents the number of cases having both values x for the row variable and y for the column variable. Correspondence Analysis associates a score to the values of each of these variables. These scores relate the two variables with a reciprocal averaging relation. In our case, for each layer, the records are the directed edges and the system of equations (6) defines the reciprocal averaging relation. Indeed, the Hub score ω_i, related to the importance of the i-th node (or time point), is computed as the weighted sum of the Authority scores θ_j of the nodes j that are "visible" from i along all the commodity series. The weight associated with each visible node j is the product of the element of the transition probability tensor $\mathcal{H}$ between nodes i and j times the Type score γ_k of the layer in which the link is present. The Authority score θ_j of node j is, instead, the weighted sum of the Hub scores ω_i of the time points i that "see" node j. The weight associated with each node i is the product of the element $a_{j|ik}$ times the Type score γ_k of the layer in which the link is present. Finally, the Type score of commodity layer k is the sum, over all pairs of nodes (i, j) connected in layer k, of the product between the Hub score ω_i with the Authority score θ_j and with the element of the transition probability tensor $\mathcal{R}$ between nodes i and j.

This approach allows us to study through the use of topological measures even non-stationary time series which may present phenomena like long-range memory and which are likely to lead to phases of market instability. Here, the tensor decomposition is instrumental when we work with multiple networks. The resulting centralities associated to time stamps recognize, in fact, increasing synchronisation phases of the system since Authority and Hub scores reveal not only whether commodity price co-move but also the direction of the co-movement towards maxima or minima, thus signaling potential abrupt transitions in the behavior of the underlying system. Indeed, the presence of a link between two nodes is a function of both the return time distribution, defined as the time required by the system to visit the same state from which it started without visiting it in between epochs, and of the roughness of the series in the basin defined by the two time stamps. In other words, the higher the return time and the lower the standard deviation of the series, the higher the probability that two time stamps distant in time will be connected by a link. Hence, time periods associated with highly connected nodes in the multilayer networks will be those representing spikes in most of the series, surrounded by observations with a low standard deviation. Moreover, to show how a different synthetic indicator would have performed to the same task, we have provided an additional comparison analysis in the Appendix (see Figure A.2) which takes into account the largest eigenvalues of the correlation matrix of the commodity price series.

Figure 3 shows the work-flow of the analysis. Univariate time series (see panel A) are transformed into binary directed networks through the direct visibility algorithm presented in Equation (1) (see panel B). Such adjacency matrices are then stacked into a tensor $\mathcal{V} \in \mathbb{R}^{T \times T \times K}$ (see panel C), which is decomposed as the outer product of three vectors representing Hub, Authority and Type scores, respectively (see panel D), using Equations (6).

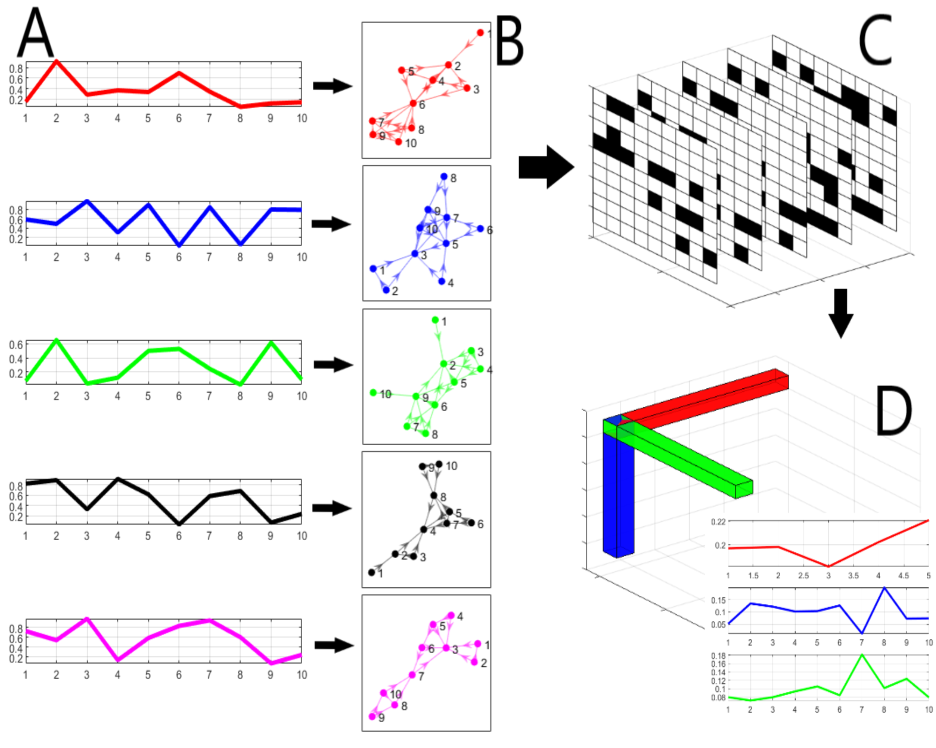

Figure 3: Work-flow of the analysis. The figure shows the steps introduced for creating our commonality index which account for both the temporal and cross-sectional patterns. The commodity time series (panel A) are transformed into graphs by means of the Directed Visibility algorithm (panel B). Then, the 3-order tensor is obtained by staking the adjacency matrices of each commodity layer (panel C). Finally, tensor decomposition is applied to extract relevant features of its relationships and build the Authority, Hub and Type centrality scores (panel D).

2.3.1 Inspecting the TOPHITS Algorithm

To inspect the functioning of the probabilistic TOPHITS algorithm, we propose an example based on simulated time series. First, we illustrate the difference between the centrality measures obtained from the two dimensional probabilistic HITS algorithm, in which we exclude the commodity layer dimension, and the simple in-(out-) degree values. Secondly, we show how the Hub and Authority scores obtained from the TOPHITS algorithm vary as long as the time series co-move.

Suppose that we have a single time series transformed into a visibility graph according to Equation (1). We aim to summarize the information contained into its adjacency matrix with two scores, namely the Hub and Authority scores obtained from the transition probabilities of the Markov chain among time stamps. For this visibility single-layer network we compute the (bivariate) conditional frequencies $\mathcal{H}$ and $\mathcal{A}$ for Hubs and Authorities by normalizing the entries of the matrix $\mathbf{V}$ as follows:

$$\begin{aligned} h_{i|j} &= \frac{v_{ij}}{\sum_{i=1}^{T} v_{ij}} \quad i = 1, ..., T \\ a_{j|i} &= \frac{v_{ij}}{\sum_{j=1}^{T} v_{ij}} \quad j = 1, ..., T \end{aligned} \tag{7}$$

where $h_{i|j}$ and $a_{j|i}$ are set to $1/T$ when $v_{ij} = 0$.

We then derive the marginal probability distributions in analogy to Equations (4-5) and, as in the TOPHITS algorithm, we compute iteratively the Hub and Authority scores as:

$$\begin{aligned} \omega_i &= \sum_{j=1}^{T} h_{i|j}\theta_j \quad i = 1, ..., T \\ \theta_j &= \sum_{i=1}^{T} a_{j|i}\omega_i \quad j = 1, ..., T \end{aligned} \tag{8}$$

Notice that the HITS algorithm produces rankings that rely on a larger amount of information than the ones obtained using only the in-(out-) degree values which account only for the number of first order neighbors. In fact, solving Equations (8) requires the use of iterative methods in which node i will be considered as an important Hub if it is a neighbor of a node j which is important in terms of Authority, and vice versa. This feedback feature of the HITS algorithm makes it a tool capable of assigning a ranking to each node according to first order information (as the degree centrality does), as well as higher order- or system- wide interdependencies. Thus, in the visibility context, the self-reinforcement mechanism (see Battiston, Puliga, et al., 2012; Flori et al., 2019) between Hub and Authority centralities can reveal the transition between different dynamic phases since the more a maximum (minimum) of a time series is visible from (see) other minima (maxima), the higher is its Authority (Hub) score and, therefore, its influence on the intensity of the transition of the system.

Then, in order to compare the rankings produced by the normalized in-(out) degree against the Hub and Authority scores, we report in Figure 4 the dynamics of a simulated time series with 15 time stamps along with the associated centrality scores. Links between nodes are reported as arrows. First, notice that node $t = 10$ has the highest values of both in-degree and Authority and it is also the global maximum in the sample. Secondly, while $t = 6$ and $t = 12$ display the same in-degree values (dark red bars), the former has a higher Authority score (light red bars), which is due to fact that such node is, on average, connected with time nodes that have higher Hub scores (light blue bars), as reported in the insert plot of Figure 4. Hence, quite high values of Hub scores followed by high values of Authority scores suggest the beginning of an upward trend in the underlying time series, which is thus emphasized by the mutual reinforcement of these centrality measures.

Next, we assess how the Hub and Authority scores behave when multiple time series co-move. This example aims to shed light on the ability of the proposed technique to

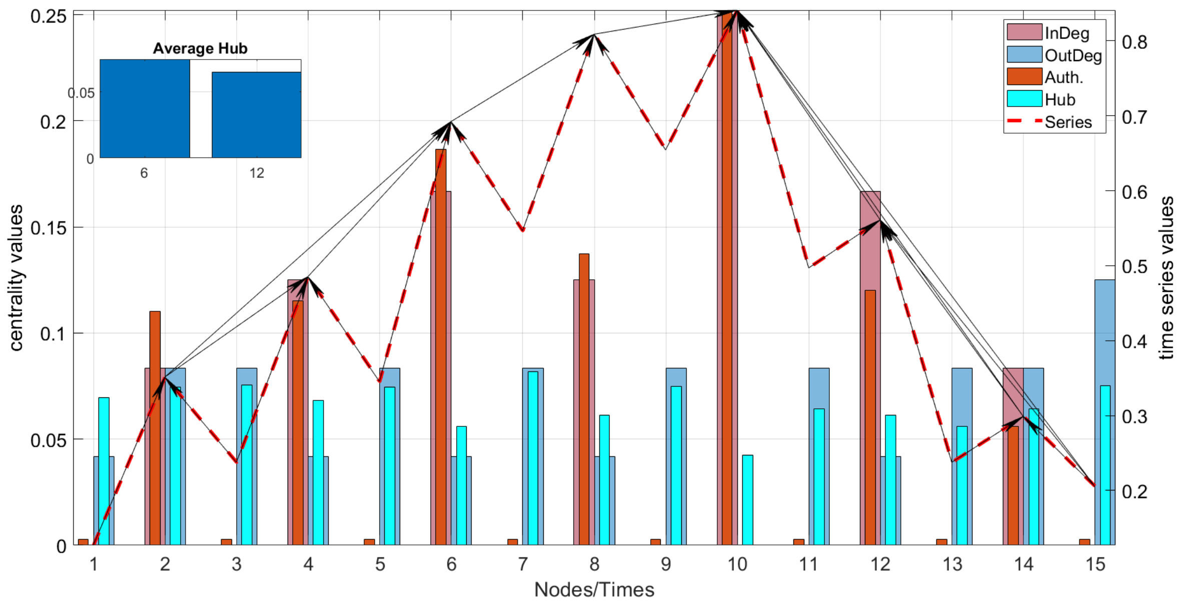

Figure 4: In- and out-degree versus Hub and Authority scores. The figure shows the normalized in- and out-degree measures for each node compared with the Hub and Authority scores computed through the HITS algorithm. The figure reports the simulated time series as a red dashed line, while black arrows represent the links obtained with the visibility graph. Blue bars represent the out-degree (darker) and the Hub ranking (lighter). Red bars represent the in-degree (darker) and the Authority ranking (lighter). The insert plot shows the average Hub values of the neighbours of nodes 6 and 12, respectively.

catch co-movements in the time series by producing higher scores in the case in which series follow a similar dynamics. Specifically, Figure 5 shows, in the left panel, two anti-correlated time series (red lines) and the corresponding Hub and Authority values (blue and orange bars, respectively). Instead, the right panel reports Hub and Authority scores when the series co-move in the same direction. For instance, note how the Authority scores, for series that co-move with opposite directions, are typically lower than those in the case of aligned co-movements, since the dynamics of such scores are reinforced when multiple series have coordinated behaviors. Moreover, for anti-correlated series, the difference between the Hub and Authority scores in each time stamp is smaller with respect to the case of positively correlated series since there is not a clear common trend reinforcing the topological properties of the time nodes. This example suggests that by applying a tensorial approach, the characteristics of multiple time series can be summarized by the Hub and Authority scores, which reveal, in a multivariate space, how such series behave not only with respect to their own dynamics, but also with regards to cross-patterns among the series.

2.4 Granger Causality Analysis

A key challenge of this paper is to reconstruct the relationships between climate-related and financial dimensions. We rely on Granger causality (Granger, 1969) to estimate the intensity of lead-lag effects between the dynamics of financial systems proxied by the FSI, the topological indicators of commodity co-movements and climate-related variables.

More formally, let $\mathbf{x}_t = x_{1,t}, x_{2,t}, .., x_{Z,t}$, with $t = 1, ..., T$, a Z-dimensional stationary time series of length T. The definition of the conditional Granger causality index (CGCI) from a driving variable x_i to a response variable x_j involves two vector autoregressive

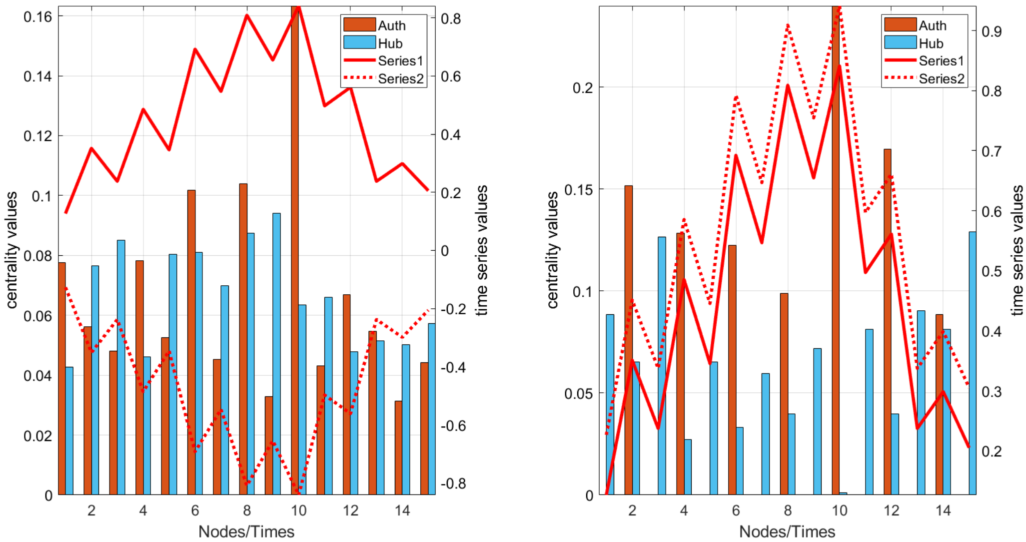

Figure 5: TOPHITS Hub and Authority scores for correlated and anti-correlated series. The figure shows the rankings produced by the probabilistic TOPHITS algorithm in the case when time series are anti-correlated (left panel) or in the case when they are positively correlated (right panel).

(VAR) models for x_j. The first model is the unrestricted model (U-model), given as:

$$x_{j,t} = \sum_{z=1}^{Z} (a_{jz,1} x_{z,t-1} + \ldots + a_{jz,p} x_{z,t-p}) + u_{j,t} \tag{9}$$

where p is the model order and $a_{jz,l}$ ($z = 1,..,Z$ and $l = 1,..,p$) are the U-model coefficients. The second model is the restricted one (R-model) derived from the U-model by excluding the lags of x_i. The Granger causality index (CGCI) can then be computed by the estimates of the residual variances $\hat{\sigma}_U^2$ and $\hat{\sigma}_R^2$ of the unrestricted (U-model) and restricted model (R-model) as follows:

$$CGCI_{x_i \to x_j} = \ln \frac{\hat{\sigma}_R^2}{\hat{\sigma}_U^2} \tag{10}$$

Moreover, we consider the Granger causality framework which provides a measure of the level of “autonomy” of a variable, where by autonomy we mean the degree of self-determination or “self-causation” exhibited by a variable (Seth, 2010a; Seth, 2010b). Hence, instead of testing whether the prediction error of x_j is reduced by including past observations of x_i, the Granger autonomy (GA) determines whether the prediction error of x_j is reduced by the inclusion of its own past values, given a set of external variables x_i with $i \neq j$. Basically, a variable x_j is Granger autonomous if its own past states allow the prediction of its future states over and above predictions based on past states of a set of other external variables. In other words, a variable is Granger autonomous to the extent that it is dependent on its own history and that these dependencies are not accounted for by external factors.

Formally, x_j is Granger autonomous if the coefficients $a_{jz,l}$ ($z = 1,..,Z$ and $l = 1,..,p$) are jointly significantly different from zero. As with Granger causality, Granger autonomy can be tested by performing an F-test on the null hypothesis that $a_{jz,l} = 0$, given the assumptions of covariance stationarity on the set of variables. Finally, the GA of x_j with respect to x_i is given by:

$$GA_{x_j|x_i} = \ln \frac{\hat{\sigma}_{R2}^2}{\hat{\sigma}_U^2} \tag{11}$$

where $\hat{\sigma}^2_{R2}$ is the estimate of the residual variance of the restricted model, in which we exclude the lags of x_j.

3 Results

3.1 Climate-related Variables, Commodities Co-Movements and Financial Stability

The Direct Visibility algorithm conveys a network representation for each commodity time series. Nodes, i.e., monthly observations, may present heterogeneous in-(out-) degrees, meaning that their visibility of the rest of the system may actually differ according to the underlying market dynamics which we attempt to capture with the proposed topological indicators. Figure 6 shows the aggregate network representation of the visibility graphs obtained from the commodity time series. Node color refers to the Hub centrality (see Kleinberg, 1999), while node size is proportional to the Authority centrality. In our sample, nodes representing periods around the global financial crisis are the most important in terms of the Authority score, while nodes with high Hub centrality values represent months prior to the crisis. Generally speaking, this finding means that in such intervals the commodity market experiences a discontinuity point, which affects most of the price series. In other words, for each time series a few nodes along the sample period reach a very high visibility. These nodes are monthly observations that stand for substantial deviations from their neighborhood, thus representing periods of utmost importance for scrutinizing market dynamics and instability.

Figure 7 exhibits the temporal evolution of the Hub and Authority scores, namely ω and θ along with the behavior of the FSI, which describes the stability of the financial system. The first part of the sample, from mid-1990 to the beginning of the new millennium, shows an almost stable behavior of all three indicators. From 2005, instead, we observe an increasing pattern for ω and θ that culminates around the outbreak of the global financial crisis, indicated by the peak of the FSI. Hence, the market euphoria characterizing the boom period prior to the global financial crisis translated into higher levels of co-movements between commodity price series, represented by the increase of both the Hub and Authority scores. Then, the eruption of the global financial crisis in 2008-2009 coincides with a sharp decrease in the level of the Authority, while the level of the Hub remains high approximately until 2011 when the crisis effects are absorbed by the markets and the FSI drops to negative values. This trajectory seems, therefore, to support the ability of the proposed topological indicators to correctly map market dynamics in terms of Hub and Authority scores, whose mutual reinforcement thus appears to contribute to a better identification of periods of financial instability.

As a further step we perform a cross-correlation analysis to investigate if the centrality measures embed some information on the dynamics of the FSI. In particular, we first compute the deviation of the FSI, Hub and Authority scores from their long-run behavior using a moving window of three years. Thus, the cross-correlation analysis reveals if the Hub and Authority deviation from their long-run trend have a lagged or a leading role on the deviation of the FSI. Hence, we apply the cross-correlation function (ccf) between pairs of time series computed as the product-moment correlation of lags between the series:

$$r_{\tilde{\omega}(\tilde{\theta}),}(p) = \frac{c_{\tilde{\omega}(\tilde{\theta}),\tilde{F}SI}(p)}{\sqrt{c_{\tilde{\omega}(\tilde{\theta}),\tilde{\omega}(\tilde{\theta})}(0)\, c_{\tilde{F}SI,\tilde{F}SI}(0)}} \tag{12}$$

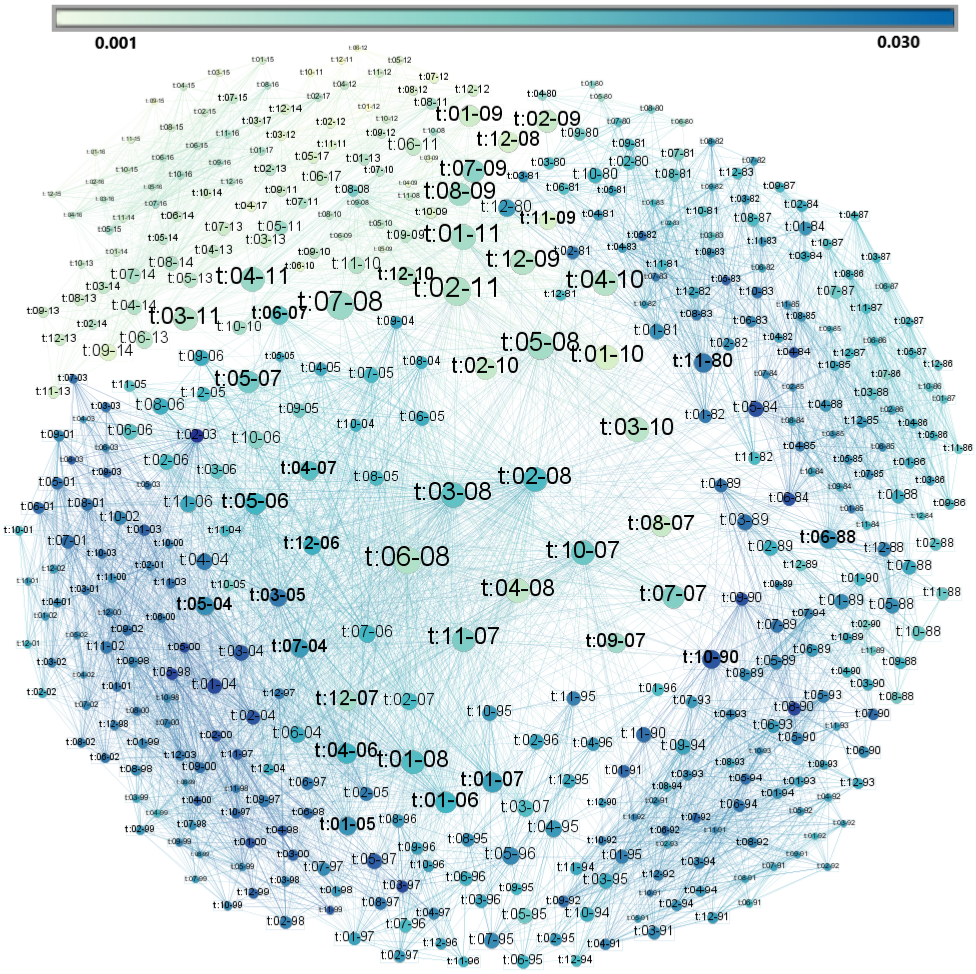

Figure 6: Aggregate network visualization of commodity visibility graphs. Each node represents a time period labeled with the corresponding time ticker, while links represent visibility between nodes. Node size is proportional to Authority centrality, while the color intensity is proportional to the Hub centrality. All measures are computed on the aggregate network. Link size is proportional to the average number of links connecting adjacent nodes in different series. Visualization is obtained by employing the Fruchterman-Reingold algorithm. Node labels represent time stamps and are proportional to node size.

where $c\,(p)$ is the cross-covariance function at lag p defined as:

$$c_{\tilde{\omega}(\tilde{\theta}),\tilde{F}SI}\,(p) = \frac{1}{N}\sum_{t=1}^{N-p}\left(\tilde{\omega}(\tilde{\theta})_t - \overline{\tilde{\omega}(\tilde{\theta})}\right)\left(\tilde{F}SI_{t+p} - \overline{\tilde{F}SI}\right); p \geq 0 \tag{13}$$

$$c_{\tilde{\omega}(\tilde{\theta}),\tilde{F}SI}\,(p) = \frac{1}{N}\sum_{t=1}^{N+p}\left(\tilde{\omega}(\tilde{\theta})_t - \overline{\tilde{\omega}(\tilde{\theta})}\right)\left(\tilde{F}SI_{t-p} - \overline{\tilde{F}SI}\right); p < 0 \tag{14}$$

and the term $\tilde{\omega}(\tilde{\theta})$ indicates that we perform cross-correlation between the difference of the Hub score ($\tilde{\omega}$) from its three year moving window and the difference of the FSI from its long-run behavior ($\tilde{F}SI$) and between the Authority difference ($\tilde{\theta}$) and the FSI difference, separately. Variables with upper bars stand for average values.

Figure 8 (left panel) shows the cross-correlation coefficients between the Hub score deviation from its long-run trend and the FSI deviation, while Figure 8 (right panel) refers to the cross-correlation between the Authority score deviation and the FSI deviation. Notice that the cross-correlation between the Hub score and the FSI is positive and statistically significant for negative lags of the latter variable, meaning that an above average value of the FSI deviation form its long-run trend is likely to lead an above

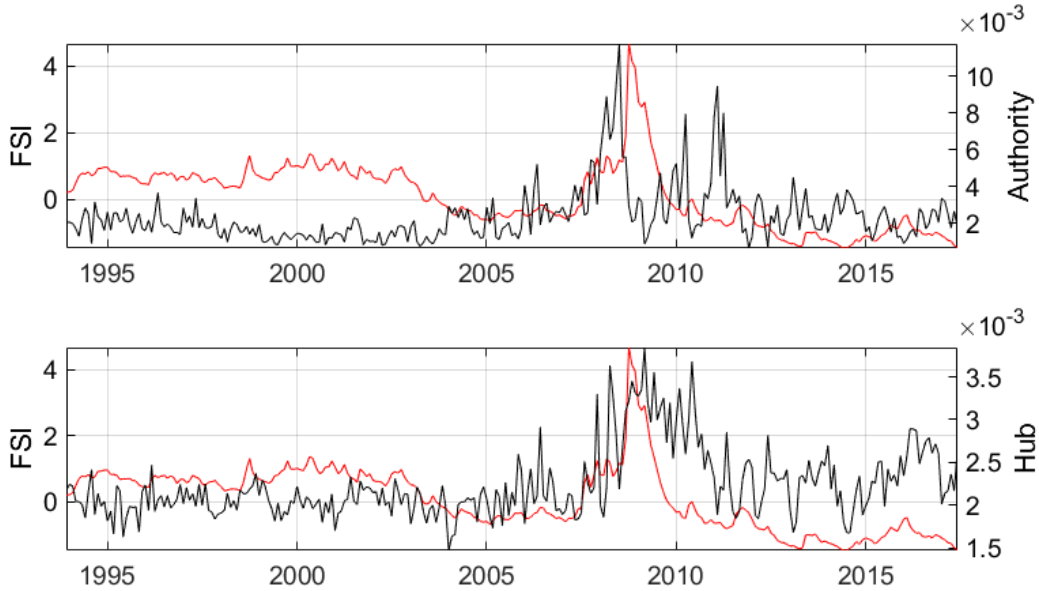

Figure 7: Hub and Authority scores along with the FSI. The figure shows the Authority score (top panel) and the Hub score (bottom panel) indicated by the black lines together with the FSI, which is reported in red.

average value of the Hub score deviation and, symmetrically, a below average value of the FSI deviation is associated with a probable below average value of the Hub score up to 6 months of delay. On the other hand, a positive value of the Hub score will influence negatively the dynamics of the FSI from 8 to 18 months in advance. The cross-cross correlation coefficient between the Authority deviation and the FSI deviation, which reaches a value higher than 0.5, shows that an increasing deviation of this centrality measure from its long-run behavior anticipates and increasing deviation of the FSI, which occurs approximately with a delay of three months. All in all, this analysis suggests that an increase of the Authority deviation or a decrease in the Hub deviation anticipate an increasing distance of FSI values from its long-run trend, thus signaling an unstable phase for financial markets.

3.2 Transmission Mechanisms within the Climate-Finance Nexus

In order to shed light on the causality nexus between climate-related variables, commodity co-movements and financial stability we perform Granger causality analysis, which allows the investigation of the causality mechanisms among the variables by inferring the functional connectivity in the underlying system.

A meaningful application of Granger causality analysis requires that the variables present covariance stationarity and that the model describes the data in a statistically satisfactory manner. Covariance stationarity requires that the first and second statistical moments (mean and variance) of each variable do not vary with time, otherwise the econometric model may contain so-called "spurious regression" results. Therefore, we assess deviations from the covariance stationary hypothesis by testing for unit roots within the data employing the augmented Dickey-Fuller (ADF) test. The intuition behind this test is that if a variable is covariance stationary it will exhibit a tendency to return to a constant mean (or deterministically trending). Basically, large values will tend to be followed by smaller values, and small values by larger values. We find that our variables are non-stationary, therefore we first differentiate all the variables obtaining $x'_{i,t} = x_{i,t} - x_{i,t-1}$. This step allows us to study the causality relationships among changes in variables rather

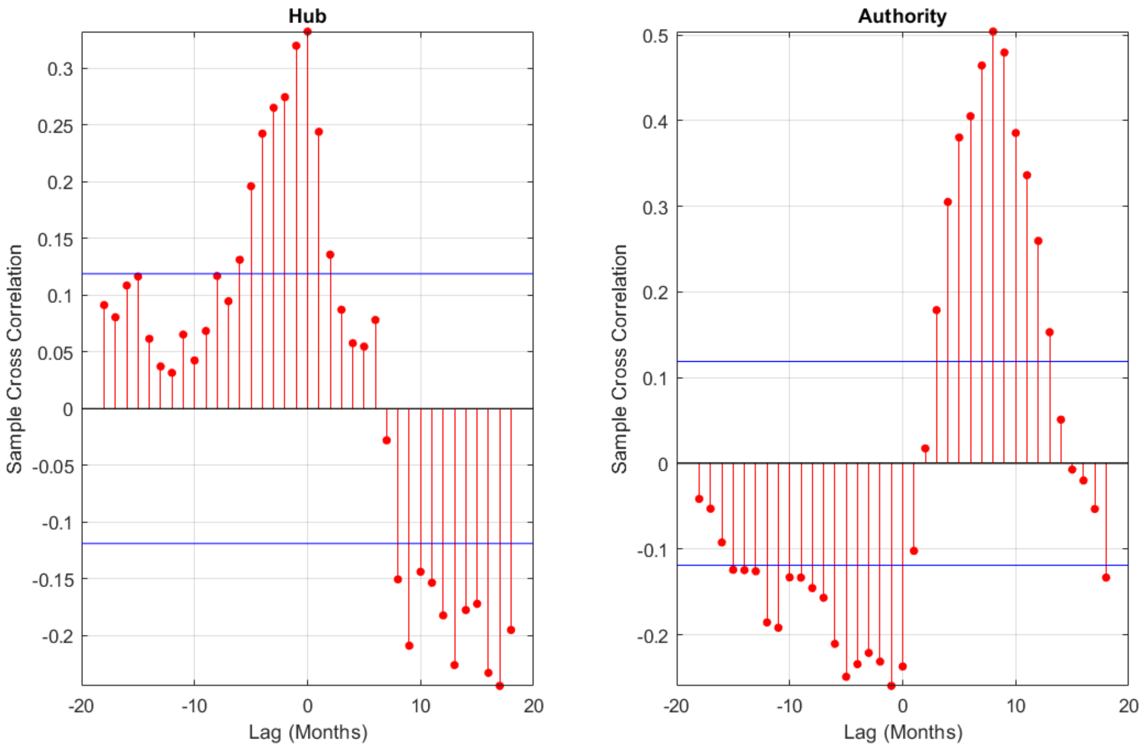

Figure 8: Hub and Authority scores cross-correlations with FSI. The figure shows the Hub score cross-correlation with the FSI (left panel) and the Authority score cross-correlation with the FSI (right panel). Blue lines indicate the upper and lower cross-correlation confidence bounds assuming uncorrelated series. All the variables have been detrended from their long-run behavior using a three year moving window. Lags represent months.

than among the variables *per se*. Secondly, the estimation of these econometric models requires the inclusion of a parameter representing the number of time-lags (p), i.e., the model order. Too few lags can lead to a poor representation of the data, whereas too many can lead to problems of model estimation in finite samples. To specify the model order, we rely on the Akaike information criterion ($AIC = \ln(\det(\Sigma)) + \frac{2pZ^2}{T}$), where Σ is the variance-covariance matrix. In this way, we balance the variance accounted for by the model against the number of coefficients to be estimated. We compute the AIC per $p = 1, ..., 24$ and we find that the best model in our sample is the one with $p = 4$ lags. In the Appendix we also report the Granger causality coefficients for $p = 2, 3, 5$ lags.

Table 1 shows the values of the Granger causality index (CGCI) along with their P-values in parenthesis. The influence direction is from columns to rows. Moreover, the table also reports some measures of the regression validity, such as the adjusted sum square error and the Durbin-Watson test on the regression residuals. Finally, in the last row of Table 1, we show the Granger autonomy of each variable. Figure 9, instead, exhibits the Granger causality network obtained by fixing a significance level for the P-value at 0.10 along with the Granger autonomy coefficients. Figure 9 shows that changes in climate-related variables, such as the wind directions (V-wind and U-wind) along with the atmospheric pressure (Press.) Granger cause changes in Hub and Authority scores, which are mutually linked with changes in FSI. In parallel, the P-values reported in Table 1 and associated with the Granger causality of Hub, Authority and FSI on the climate-related series are, on average, the highest. As expected, while the Hub and Authority scores obtained from commodity time series are influenced by climate-related variables, the opposite is not true and, obviously, for FSI this is even more evident. For instance, this result can be interpreted in the light of the El-nino-Southern Oscillation (ENSO), which periodically causes anomalous shifts in the atmospheric pressure. Although ENSO events arise in the

Pacific Ocean, their effects have global impacts and influence commodity productions (see Brunner, 2002), directly (as for crops) and undirectly (as for mining firms, energy supply and waterway transportation).

	Hub	**Authority**	**FSI**	**Rainfall**	**Temp.**	**Press.**	**V-wind**	**U-wind**
Hub		0.058 (0.006)	0.066 (0.003)	0.021 (0.270)	0.009 (0.679)	0.048 (0.018)	0.036 (0.064)	0.023 (0.235)
Authority	0.080 (0.001)		0.035 (0.072)	0.014 (0.476)	0.011 (0.602)	0.056 (0.008)	0.004 (0.927)	0.034 (0.079)
FSI	0.040 (0.043)	0.070 (0.002)		0.023 (0.218)	0.005 (0.853)	0.010 (0.643)	0.004 (0.899)	0.010 (0.640)
Rainfall	0.009 (0.717)	0.027 (0.157)	0.006 (0.819)		0.019 (0.316)	0.011 (0.623)	0.028 (0.140)	0.011 (0.598)
Temp.	0.003 (0.947)	0.012 (0.550)	0.023 (0.233)	0.017 (0.366)		0.013 (0.537)	0.005 (0.882)	0.006 (0.842)
Press.	0.008 (0.749)	0.010 (0.637)	0.010 (0.633)	0.010 (0.647)	0.006 (0.813)		0.015 (0.461)	0.003 (0.955)
V-wind	0.016 (0.413)	0.000 (1.000)	0.008 (0.732)	0.015 (0.732)	0.001 (0.465)	0.022 (0.246)		0.028 (0.142)
U-wind	0.025 (0.188)	0.008 (0.731)	0.010 (0.660)	0.007 (0.785)	0.013 (0.509)	0.012 (0.564)	0.015 (0.443)	
Adj R^2	0.318	0.237	0.050	0.194	0.222	0.185	0.242	0.244
D-W test	0.584	0.248	0.922	0.453	0.549	0.552	0.426	0.760
G-Auton.	0.212 (0.000)	0.160 (0.000)	0.051 (0.014)	0.238 (0.000)	0.263 (0.000)	0.091 (0.000)	0.313 (0.000)	0.162 (0.000)

Table 1: Granger causality values. The table reports the results of the Granger causality analysis along with the P-values (in parenthesis) associated with the coefficients. Causality direction is from column variables to row variables. The last row represents the Granger autonomy.

Moreover, from Table 1 we notice that a change in the values of the FSI has a stronger effect on Hub rather than on Authority changes, while changes in the Authority impact more on changes of the FSI than on changes in the Hub score. We can interpret these results in the following way: a positive change in the FSI value which indicates a growing market instability induces a positive change in the Hub score which signals that commodity prices are co-moving on a downward trend, while a change in the Authority value which signals commodity co-movement on an upward trend induces a subsequent positive change in the FSI since it increases the likelihood of market distress when price levels are no longer sustainable. The Granger autonomy analysis reinforces these findings, since the most autonomous variables are the climate-related ones, while the FSI is the less autonomous as it has the lowest degree of self-determination in this system.

Finally, we enrich the analysis on the nexus between FSI and the topological indicators by analyzing the direction of causality, i.e., mean spillover effects, through the variant of the Granger causality test introduced by Toda and Yamamoto (1995). This testing does not require for cointegration and it is robust even in the presence of a unit root in the time series, thus implying that there is no need to transform the original series to obtain stationarity and therefore any loss of information due to differencing is avoided. More generally, this approach could be interpreted as a long-run causality test (see, e.g., Nazlioglu and Soytas, 2011; Nazlioglu, Soytas, and Gupta, 2015). Specifically, we run a VAR $(p + dmax)$ model with p as the optimal lag and $dmax$ as the maximum integration degree of the series; then, standard Wald tests for the null of non-Grange causality is performed by imposing zero restrictions on the first p lags. Results indicate that the Lagrange Multiplier statistics (p-values in parenthesis) for causality of Hub and Authority to FSI are significant and equal to 5.4 (0.02) and 6.4 (0.09) respectively, while the reverse relationships are 0.37 (0.54) and 16.9 (0.00075) respectively, with the latter being very strong and significant. The mean spillover test provides therefore supporting evidences of

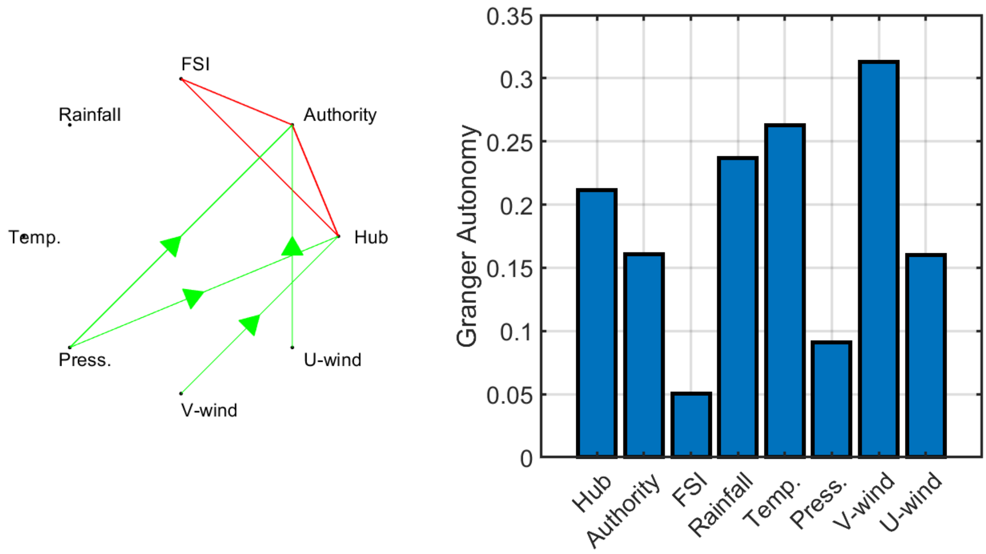

Figure 9: Granger causality and Granger autonomy. The figure shows the Granger causality network with links present if below a P-value of 0.10 (left panel) and the Granger autonomy (right panel). Green arrows report the direction of the Granger causality, while red edges refer to Granger causality in both directions.

information flow from FSI and the topological measures, and vice versa.

As regards financial stability and systemic risk assessment, we thus support the importance of an evaluation based on panel observations, as suggested by the Macroprudential Policy Framework which contributed to motivate our investigation framework. As pointed out by Borio (2011), indeed, macroprudential is an orientation or perspective of regulatory and supervisory arrangements which calibrate supervision from a systemwide or systemic perspective, rather than from that of the safety and soundness of single institutions on a stand-alone basis. Therefore, regulators can benefit from the provision of few synthetic indicators of instability, such as those proposed in our work, that could help them to design appropriate policy actions to timely respond against climate-related challenges that may impact on the stability conditions of financial systems. Our approach is able to map the panel dimension of commodity time series and extract meaningful information on commodity price co-movements, which we show to be influenced by climate-related variables and, more interestingly, to be mutually related with FSI, hence with an indicator of financial stability in capital markets. In particular, major variations in climate-related variables are promptly captured by the topological indicators of price co-movements, which can be employed to synthesize this information and then include it in an econometric setup for assessing financial stability in wider financial markets.

3.3 Short-run dynamics via impulse response analysis

Finally, to assess how our variables of interest react to short-run shocks, we perform an impulse-response analysis on Hub, Authority and FSI. We rely on the procedure proposed by Jordà (2005) to generate the estimation of the local projections at each period rather than the entire forecast horizon. This approach has been shown to be more robust to misspecification of the unknown data generative process and allows appropriate joint and point-wise inference based on standard errors from traditional heteroskedastic and autocorrelation consistent regressions.

Figure 10 shows the impulse response related to the financial stability conditions (i.e., FSI) and our proposed topological measures mapping commodities price co-movements (i.e., Hub and Authority). Note how each variable significantly reacts to shocks occurring

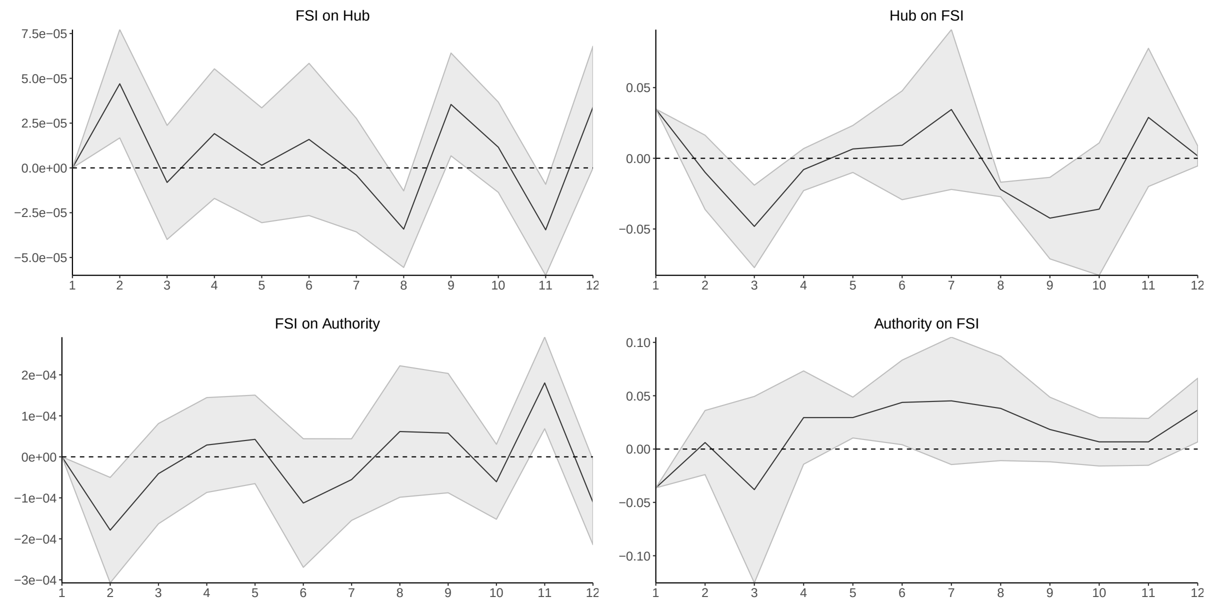

Figure 10: Impulse response analysis. The response is calculated with a local-linear projection with 4 lags. The analysis considers an impulse of one standard deviation shock of the variable of interest (i.e., Hub, Authority and FSI). The gray area refers to a confidence interval of 95%.

in one of the other variables only in the short-run (about 1-2 months). Capital and commodity markets result to be connected and prone to spillover effects from and to price movements occurring in the underlying financial instruments, although, as expected, these effects are short-lived. More specifically, both Hub and FSI present a positive response to an impulse in the other dimension, while a negative reaction occurs for impulses within the pair of Authority and FSI, meaning that an impulse that increases Hub centrality implies that also the overall level of instability rises, while an increase in the Authority centrality reduces FSI but only in the short-run. Hence, by interpreting Hub and Authority centralities as time-stamps in which commodity price series co-move respectively into minima and maxima in terms of market prices, the impulse response analysis seems to suggest that shocks favoring synchronized market downturns of commodity prices are likely to coexist with immediately subsequent periods of overall market instability, while the opposite occurs for an impulse affecting commodity co-movements during the initial stages of positive market price phases. In line with these findings, an impulse that increases the FSI generates a rise in the Hub centrality and a drop in the Authority during subsequent periods, thus supporting the nexus between capital market stability conditions and commodity price co-movements. However, this nexus is statistically significant only in the short run and is absorbed quickly by financial markets.

4 Conclusion

This work aims at defining the nexus between climate-related variables, commodities price co-movements and financial stability which can help policymakers to design appropriate policy actions to timely respond to climate-related challenges. To disentangle transient phases of critical states leading to financial instability, we propose a multidimensional graph-theoretical approach that maps commodity price co-movements into network centrality indicators and that takes into account both the presence of correlated behaviors and the directionality of these co-movements. In so doing, we exploit information contained into centrality measures computed through a tensor approach applied on a multilayer visibility network. This step is instrumental for obtaining synthetic scores that characterize the role of different nodes (time stamps) during phases of market downturns or upturns, unveiling therefore the onset of financial instability. We thus combine a visibility graph algorithm, which has been proven to maintain relevant time series information in a consistent way, with a tensor decomposition, which is instrumental to extract a few synthetic indicators of directional co-movements that can then be employed to analyze market stability conditions over time observations.

Specifically, we rely on the visibility graph framework to develop an algorithm that converts a commodity price time series into a directed graph that inherits some structural properties of the original data. Then, we build a multilayer network formed by stacking together each commodity visibility graph and we apply tensor decomposition to extract information from it. We then propose to synthesize the extent of co-movements with a few synthetic indicators of network centrality, which we show to be able to identify periods of market instability. We notice that relevant price changes affecting several commodity time series correspond to nodes with high scores of the proposed centrality measures. These indicators convey information on the return time distribution of the multivariate time series and reveal the extent of upwards and downwards co-movements among commodity prices.

Then, we include these centrality measures into an econometric model to study the relationships between such topological measures, the stability conditions of financial systems and climate-related dimensions. Our approach reveals that the proposed topological indicators react to variations in climate-related conditions and supports the existence of a nexus with financial stability. Hence, this econometric investigation can contribute to an explainable forecasting and critical analysis of the transmission mechanisms that connect climate conditions, macroeconomics and financial systems.

Despite the merits of our approach to unveil the nexus between climate-related variables and financial stability through the impact the former have on commodity prices, we are aware of its main limitations. First, to show the functioning of a very general framework for investigating the relationships between climate-related conditions, commodities and financial systems, we opt for a broad representation of climate conditions, which does not appropriately take into account all climate and environmental dimensions specifically affecting certain commodities. Second, due to the level of aggregation of our data, we have been forced to average all climate-related variables across coordinate grid points, thus ignoring cross sectional and geographical aspects of the impact of climate-related phenomena on local commodity markets. Third, our paper relies on monthly observations of commodity prices. Also for this reason, we do not study phases of market instability that occur at higher frequencies. Finally, the construction of a visibility graph is intended to provide a binary adjacency matrix of the links connecting time stamps. Since links are not weighted by the differential value assumed by the connected pairs of nodes in the series, our approach does not directly inherit information on price jumps to be used, for instance, for the analysis of extreme events.

Our approach does not assume any specific functional form for the data generating processes, therefore it can be potentially applied to any source of data. This comes at the cost of a lack of statistical test for assessing the robustness of the links, which may be influenced by the presence of noise in the series. To mitigate this issue, future works may address statistical significance by carrying out bootstrapping and permutation tests based on null models for network configurations ensembles.

Declaration of Competing Interest

The authors report no declarations of interest.

References

Ahmadlou, Mehran, Hojjat Adeli, and Anahita Adeli (2010). "New diagnostic EEG markers of the Alzheimer's disease using visibility graph". In: *Journal of neural transmission* 117.9, pp. 1099–1109.

Alley, Richard B et al. (2003). "Abrupt climate change". In: *Science* 299.5615, pp. 2005–2010.

Avdjiev, Stefan, Paolo Giudici, and Alessandro Spelta (2019). "Measuring contagion risk in international banking". In: *Journal of Financial Stability*.

Battiston, Stefano, Antoine Mandel, Irene Monasterolo, Franziska Schütze, and Gabriele Visentin (2017). "A climate stress-test of the financial system". In: *Nature Climate Change* 7.4, p. 283.

Battiston, Stefano, Michelangelo Puliga, Rahul Kaushik, Paolo Tasca, and Guido Caldarelli (2012). "Debtrank: Too central to fail? financial networks, the fed and systemic risk". In: *Scientific reports* 2, p. 541.

Baumeister, Christiane and Lutz Kilian (2014). "Do oil price increases cause higher food prices?" In: *Economic Policy* 29.80, pp. 691–747.

Becken, Susanne and John E Hay (2007). *Tourism and climate change: Risks and opportunities*. Vol. 1. Multilingual Matters.

Borio, Claudio (2011). "Implementing a macroprudential framework: Blending boldness and realism". In: *Capitalism and Society* 6.1.

Brack, Duncan (2013). *International trade and climate change policies*. Routledge.

Brohan, Phillip, John J Kennedy, Ian Harris, Simon FB Tett, and Phil D Jones (2006). "Uncertainty estimates in regional and global observed temperature changes: A new data set from 1850". In: *Journal of Geophysical Research: Atmospheres* 111.D12.

Brown, Molly E and Christopher C Funk (2008). "Food security under climate change". In: *Science* 319.5863, pp. 580–581.

Brunner, Allan D (2002). "El Nino and world primary commodity prices: warm water or hot air?" In: *Review of Economics and statistics* 84.1, pp. 176–183.

Carney, Mark (2015). "Breaking the Tragedy of the Horizon–climate change and financial stability". In: *Speech given at Lloyd's of London* 29, pp. 220–230.

Collins, Matthew et al. (2013). "Long-term climate change: projections, commitments and irreversibility". In:

Dafermos, Yannis, Maria Nikolaidi, and Giorgos Galanis (2018). "Climate change, financial stability and monetary policy". In: *Ecological Economics* 152, pp. 219–234.

Dietz, Simon, Alex Bowen, Charlie Dixon, and Philip Gradwell (2016). "'Climate value at risk'of global financial assets". In: *Nature Climate Change* 6.7, p. 676.

Ding, Mingzhou and Weiming Yang (1995). "Distribution of the first return time in fractional Brownian motion and its application to the study of on-off intermittency". In: *Physical Review E* 52.1, p. 207.

Donner, Reik V and Jonathan F Donges (2012). "Visibility graph analysis of geophysical time series: Potentials and possible pitfalls". In: *Acta Geophysica* 60.3, pp. 589–623.

Donner, Reik V, Michael Small, Jonathan F Donges, Norbert Marwan, Yong Zou, Ruoxi Xiang, and Jürgen Kurths (2011). "Recurrence-based time series analysis by means of complex network methods". In: *International Journal of Bifurcation and Chaos* 21.04, pp. 1019–1046.

Fan, Yun and Huug Van den Dool (2008). "A global monthly land surface air temperature analysis for 1948–present". In: *Journal of Geophysical Research: Atmospheres* 113.D1.

Farid, Mai, Michael Keen, Michael Papaioannou, Ian Parry, Catherine Pattillo, Anna Ter-Martirosyan, et al. (2016). “After Paris: Fiscal, macroeconomic, and financial implications of climate change”. In: *IMF Staff Discussion Note* 16.1.

Filip, Ondrej, Karel Janda, Ladislav Kristoufek, and David Zilberman (2016). “Dynamics and evolution of the role of biofuels in global commodity and financial markets”. In: *Nature Energy* 1.12, p. 16169.

Fischer, G, K Frohberg, ML Parry, and C Rosenzweig (1994). “Climate change and world food supply, demand and trade: Who benefits, who loses?” In: *Global Environmental Change* 4.1, pp. 7–23.

Flanagan, Ryan and Lucas Lacasa (2016). “Irreversibility of financial time series: a graph-theoretical approach”. In: *Physics Letters A* 380.20, pp. 1689–1697.

Flori, Andrea, Fabrizio Lillo, Fabio Pammolli, and Alessandro Spelta (2019). “Better to stay apart: asset commonality, bipartite network centrality, and investment strategies”. In: *Annals of Operations Research*, pp. 1–37.

Flori, Andrea, Fabio Pammolli, Sergey V Buldyrev, Luca Regis, and H Eugene Stanley (2019). “Communities and regularities in the behavior of investment fund managers”. In: *Proceedings of the National Academy of Sciences* 116.14, pp. 6569–6574.

Gabaix, Xavier, Parameswaran Gopikrishnan, Vasiliki Plerou, and H Eugene Stanley (2003). “A theory of power-law distributions in financial market fluctuations”. In: *Nature* 423.6937, p. 267.

Gao, Zhong-Ke, Qing Cai, Yu-Xuan Yang, Wei-Dong Dang, and Shan-Shan Zhang (2016). “Multiscale limited penetrable horizontal visibility graph for analyzing nonlinear time series”. In: *Scientific Reports* 6, p. 35622.

Giuzio, Margherita, Dejan Krušec, Anouk Levels, Ana Sofia Melo, Katri Mikkonen, Petya Radulova, et al. (2019). “Climate change and financial stability”. In: *Financial Stability Review* 1.

Granger, Clive WJ (1969). “Investigating causal relations by econometric models and cross-spectral methods”. In: *Econometrica: Journal of the Econometric Society*, pp. 424–438.

Greenacre, Michael (2017). *Correspondence analysis in practice*. CRC press.

Hamilton, Jacqueline M, David J Maddison, and Richard SJ Tol (2005). “Climate change and international tourism: a simulation study”. In: *Global Environmental Change* 15.3, pp. 253–266.

Heemeijer, Peter, Cars Hommes, Joep Sonnemans, and Jan Tuinstra (2009). “Price stability and volatility in markets with positive and negative expectations feedback: An experimental investigation”. In: *Journal of Economic dynamics and control* 33.5, pp. 1052–1072.

Hong, Harrison, Frank Weikai Li, and Jiangmin Xu (2019). “Climate risks and market efficiency”. In: *Journal of Econometrics* 208.1, pp. 265–281.

Hou, FZ, FW Li, J Wang, and FR Yan (2016). “Visibility graph analysis of very short-term heart rate variability during sleep”. In: *Physica A: Statistical Mechanics and its Applications* 458, pp. 140–145.

Houghton, John Theodore, Geoffrey J Jenkins, and Jim J Ephraums (1991). *Climate change*.

Howden, S Mark, Jean-François Soussana, Francesco N Tubiello, Netra Chhetri, Michael Dunlop, and Holger Meinke (2007). “Adapting agriculture to climate change”. In: *Proceedings of the National Academy of Sciences* 104.50, pp. 19691–19696.

Jones, PD, DH Lister, TJ Osborn, C Harpham, M Salmon, and CP Morice (2012). “Hemispheric and large-scale land-surface air temperature variations: An extensive revision and an update to 2010”. In: *Journal of Geophysical Research: Atmospheres* 117.D5.

Jones, PD, TJ Osborn, KR Briffa, CK Folland, EB Horton, LV Alexander, DE Parker, and NA Rayner (2001). "Adjusting for sampling density in grid box land and ocean surface temperature time series". In: *Journal of Geophysical Research: Atmospheres* 106.D4, pp. 3371–3380.

Jordà, Òscar (2005). "Estimation and inference of impulse responses by local projections". In: *American economic review* 95.1, pp. 161–182.

Kleinberg, Jon M (1999). "Authoritative sources in a hyperlinked environment". In: *Journal of the ACM (JACM)* 46.5, pp. 604–632.

Kliesen, Kevin L, Michael T Owyang, E Katarina Vermann, et al. (2012). "Disentangling diverse measures: A survey of financial stress indexes". In: *Federal Reserve Bank of St. Louis Review* 94.5, pp. 369–397.

Kliesen, Kevin L, Douglas C Smith, et al. (2010). "Measuring financial market stress". In: *Economic Synopses*.

Kolda, Tamara G and Brett W Bader (2009). "Tensor decompositions and applications". In: *SIAM Review* 51.3, pp. 455–500.

Kolda, Tamara G, Brett W Bader, and Joseph P Kenny (2005). "Higher-order web link analysis using multilinear algebra". In: *Fifth IEEE International Conference on Data Mining (ICDM'05)*. IEEE, 8–pp.

Kristoufek, Ladislav, Karel Janda, and David Zilberman (2012). "Correlations between biofuels and related commodities before and during the food crisis: A taxonomy perspective". In: *Energy Economics* 34.5, pp. 1380–1391.

Lacasa, Lucas and Ryan Flanagan (2015). "Time reversibility from visibility graphs of nonstationary processes". In: *Physical Review E* 92.2, p. 022817.

Lacasa, Lucas, Bartolo Luque, Fernando Ballesteros, Jordi Luque, and Juan Carlos Nuno (2008). "From time series to complex networks: The visibility graph". In: *Proceedings of the National Academy of Sciences* 105.13, pp. 4972–4975.

Lacasa, Lucas, Bartolo Luque, Jordi Luque, and Juan Carlos Nuno (2009). "The visibility graph: A new method for estimating the Hurst exponent of fractional Brownian motion". In: *EPL (Europhysics Letters)* 86.3, p. 30001.

Lacasa, Lucas, Vincenzo Nicosia, and Vito Latora (2015). "Network structure of multivariate time series". In: *Scientific Reports* 5, p. 15508.

Lacasa, Lucas, Angel Nunez, Édgar Roldán, Juan MR Parrondo, and Bartolo Luque (2012). "Time series irreversibility: a visibility graph approach". In: *The European Physical Journal B* 85.6, p. 217.

Lebart, Ludovic, Alain Morineau, and Marie Piron (1995). *Statistique exploratoire multidimensionnelle.* Vol. 3. Dunod Paris.

Leichenko, Robin M, Karen L O'Brien, and William D Solecki (2010). "Climate change and the global financial crisis: a case of double exposure". In: *Annals of the Association of American Geographers* 100.4, pp. 963–972.

Lucotte, Yannick (2016). "Co-movements between crude oil and food prices: A post-commodity boom perspective". In: *Economics Letters* 147, pp. 142–147.

Mattoo, Aaditya, Arvind Subramanian, Dominique Van Der Mensbrugghe, and Jianwu He (2009). *Reconciling climate change and trade policy.* The World Bank.

McKibbin, Warwick J and Peter J Wilcoxen (2002). "The role of economics in climate change policy". In: *Journal of Economic Perspectives* 16.2, pp. 107–129.

Meehl, Gerard A et al. (2007). "Global climate projections". In:

Nazlioglu, Saban and Ugur Soytas (2011). "World oil prices and agricultural commodity prices: Evidence from an emerging market". In: *Energy Economics* 33.3, pp. 488–496.

Nazlioglu, Saban, Ugur Soytas, and Rangan Gupta (2015). "Oil prices and financial stress: A volatility spillover analysis". In: *Energy Policy* 82, pp. 278–288.

Nelson, Gerald C et al. (2009). *Climate change: Impact on agriculture and costs of adaptation.* Vol. 21. Intl Food Policy Res Inst.
Ng, Michaek Kwok-Po, Xutao Li, and Yunming Ye (2011). "Multirank: co-ranking for objects and relations in multi-relational data". In: *Proceedings of the 17th ACM SIGKDD international conference on Knowledge discovery and data mining.* ACM, pp. 1217–1225.
Nordhaus, William D (1994). *Managing the global commons: the economics of climate change.* Vol. 31. MIT press Cambridge, MA.
— (2007). "A review of the Stern review on the economics of climate change". In: *Journal of Economic Literature* 45.3, pp. 686–702.
o'Brien, Karen et al. (2004). "Mapping vulnerability to multiple stressors: climate change and globalization in India". In: *Global Environmental Change* 14.4, pp. 303–313.
Orsenigo, Luigi, Fabio Pammolli, and Massimo Riccaboni (2001). "Technological change and network dynamics: lessons from the pharmaceutical industry". In: *Research policy* 30.3, pp. 485–508.
Pammolli, Fabio and Massimo Riccaboni (2002). "Technological regimes and the growth of networks: An empirical analysis". In: *Small Business Economics* 19.3, pp. 205–215.
Parry, Martin, Cynthia Rosenzweig, Ana Iglesias, Günther Fischer, and Matthew Livermore (1999). "Climate change and world food security: a new assessment". In: *Global Environmental Change* 9, S51–S67.
Piot-Lepetit, Isabelle and Robert M'Barek (2011). "Methods to analyse agricultural commodity price volatility". In: *Methods to analyse agricultural commodity price volatility.* Springer, pp. 1–11.
Plerou, Vasiliki, Parameswaran Gopikrishnan, Xavier Gabaix, H Eugene Stanley, et al. (2004). "On the origin of power-law fluctuations in stock prices". In: *Quantitative Finance* 4.1, pp. C11–C15.
Pollitt, Hector and Jean-Francois Mercure (2018). "The role of money and the financial sector in energy-economy models used for assessing climate and energy policy". In: *Climate Policy* 18.2, pp. 184–197.
Qian, Meng-Cen, Zhi-Qiang Jiang, and Wei-Xing Zhou (2010). "Universal and nonuniversal allometric scaling behaviors in the visibility graphs of world stock market indices". In: *Journal of Physics A: Mathematical and Theoretical* 43.33, p. 335002.
Reboredo, Juan C (2012). "Do food and oil prices co-move?" In: *Energy Policy* 49, pp. 456–467.
Roldán, Édgar and Juan MR Parrondo (2010). "Estimating dissipation from single stationary trajectories". In: *Physical review letters* 105.15, p. 150607.
— (2012). "Entropy production and Kullback-Leibler divergence between stationary trajectories of discrete systems". In: *Physical Review E* 85.3, p. 031129.
Seth, Anil K (2010a). "A MATLAB toolbox for Granger causal connectivity analysis". In: *Journal of Neuroscience Methods* 186.2, pp. 262–273.
— (2010b). "Measuring autonomy and emergence via Granger causality". In: *Artificial Life* 16.2, pp. 179–196.
Spelta, Alessandro, Andrea Flori, and Fabio Pammolli (2018). "Investment communities: Behavioral attitudes and economic dynamics". In: *Social Networks* 55, pp. 170–188.
Spelta, Alessandro, Andrea Flori, Nicolò Pecora, Sergey Buldyrev, and Fabio Pammolli (2020). "A behavioral approach to instability pathways in financial markets". In: *Nature communications* 11.1, pp. 1–9.
Spelta, Alessandro, Andrea Flori, Nicolò Pecora, and Fabio Pammolli (2019). "Financial crises: uncovering self-organized patterns and predicting stock markets instability". In: *Journal of Business Research.*

Springmann, Marco, Daniel Mason-D'Croz, Sherman Robinson, Keith Wiebe, H Charles J Godfray, Mike Rayner, and Peter Scarborough (2017). "Mitigation potential and global health impacts from emissions pricing of food commodities". In: *Nature Climate Change* 7.1, p. 69.

Stern, Nicholas (2008). "The economics of climate change". In: *American Economic Review* 98.2, pp. 1–37.

Stolbova, Veronika, Irene Monasterolo, and Stefano Battiston (2018). "A financial macro-network approach to climate policy evaluation". In: *Ecological Economics* 149, pp. 239–253.

Strozzi, Fernanda, Jose-Manuel Zaldıvar, Karmen Poljanšek, Flavio Bono, and Eugenio Gutierrez (2009). *From complex networks to time series analysis and viceversa: Application to metabolic networks*. Citeseer.

Tang, Jinjun, Fang Liu, Weibin Zhang, Shen Zhang, and Yinhai Wang (2016). "Exploring dynamic property of traffic flow time series in multi-states based on complex networks: Phase space reconstruction versus visibility graph". In: *Physica A: Statistical Mechanics and its Applications* 450, pp. 635–648.

Toda, Hiro Y and Taku Yamamoto (1995). "Statistical inference in vector autoregressions with possibly integrated processes". In: *Journal of Econometrics* 66.1-2, pp. 225–250.

UNDRR (2019). *Global Assessment Report on Disaster Risk Reduction 2019*.

Wang, Na, Dong Li, and Qiwen Wang (2012). "Visibility graph analysis on quarterly macroeconomic series of China based on complex network theory". In: *Physica A: Statistical Mechanics and its Applications* 391.24, pp. 6543–6555.

Wells, Victoria K, Cerys A Ponting, and Ken Peattie (2011). "Behaviour and climate change: Consumer perceptions of responsibility". In: *Journal of Marketing Management* 27.7-8, pp. 808–833.

Wheeler, Tim and Joachim Von Braun (2013). "Climate change impacts on global food security". In: *Science* 341.6145, pp. 508–513.

Whitmarsh, Lorraine (2009). "Behavioural responses to climate change: Asymmetry of intentions and impacts". In: *Journal of Environmental Psychology* 29.1, pp. 13–23.

Xie, Pingping and Phillip A Arkin (1997). "Global precipitation: A 17-year monthly analysis based on gauge observations, satellite estimates, and numerical model outputs". In: *Bulletin of the American Meteorological Society* 78.11, pp. 2539–2558.

Xu, Xiaoke, Jie Zhang, and Michael Small (2008). "Superfamily phenomena and motifs of networks induced from time series". In: *Proceedings of the National Academy of Sciences* 105.50, pp. 19601–19605.

A Appendix

Supplementary Figures

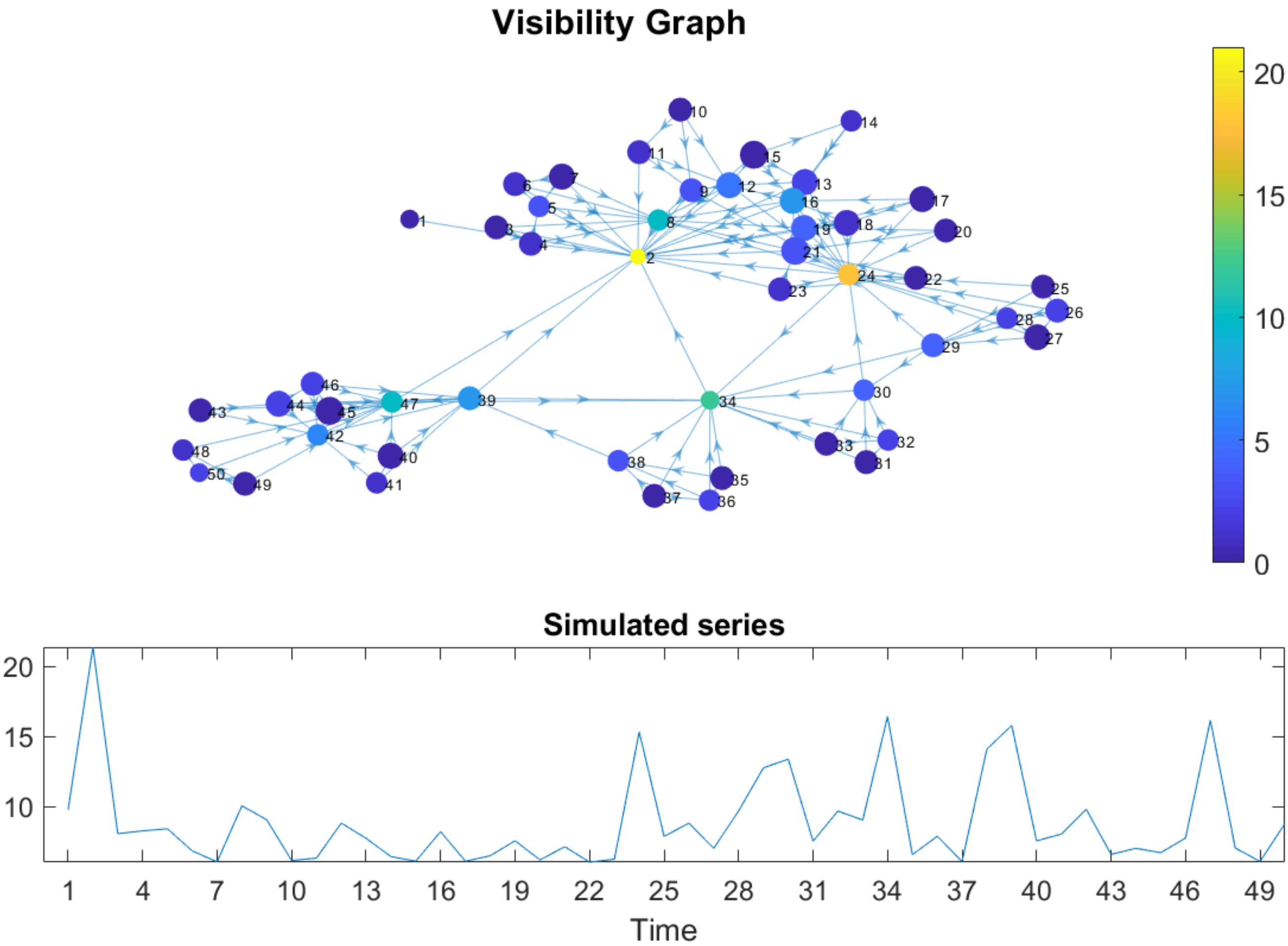

Figure A.1: Visibility Graph representation of a time series. The figure shows in the upper panel the visibility graph mapping of the simulated time series (reported in the lower panel). Node color is associated with the in-degree (reported in the colorbar), while node size is proportional to the out-degree. Local maxima of the simulated series are mapped into high in-degree nodes with yellow color (e.g., $t = 2$ or $t = 24$), while local minima are mapped into high out-degree nodes with larger size (e.g., $t = 10$ or $t = 15$).

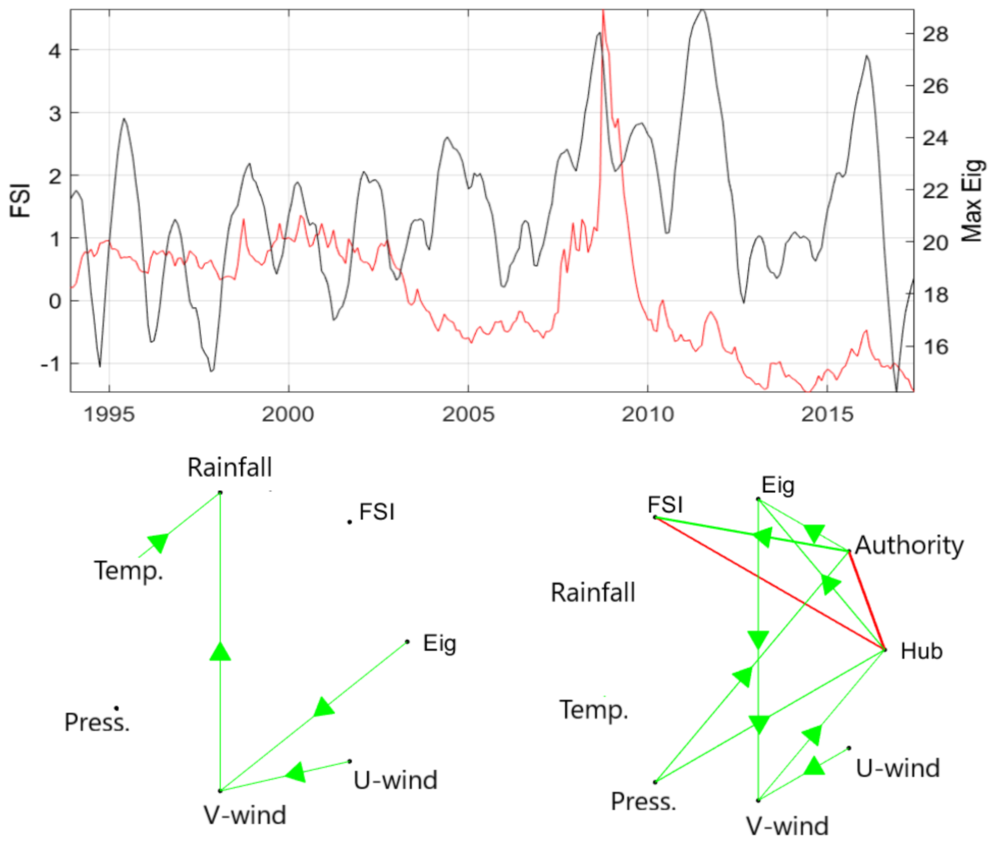

Figure A.2: Correlation matrix eigenvector dynamics.The figure shows in the upper panel the value of the largest eigenvector of the correlation matrix obtained from commodity price series (in black color) against the FSI (in red). To compute Eig we use a moving window of 25 weeks. The bottom left panel reports the Granger causality network where the economic dimension of the data is given by the FSI and Eig only. The bottom right panel shows the Granger causality network in which together with Hub and Authority, also Eig is included. Notice how while both Eig and FSI peak synchronously during the outburst of 2007-08 financial crisis, Eig presents other peaks not aligned with the FSI jumps. From the bottom left panel, notice also how the link from Eig to V-wind represents an evident spurious relationship (at significance level of P-value of 0.10, green arrows report the direction of the Granger causality, while red edges refer to Granger causality in both directions). From the right bottom panel, notice how only the Authority and Hub scores show statistically significant Granger causality links towards FSI.

Supplementary Tables

In this Appendix we report the results of the sensitivity analysis of the Granger causality coefficients as long as the lag order p varies. Tables A.1, A.2 and A.3 in particular show the Granger causality coefficients obtained for $p = 2, 3, 5$ lags, respectively. Estimated coefficients display statistical robustness against different values of p, thus reinforcing the causality relationships found among variables.

	Hub	**Authority**	**FSI**	**Rainfall**	**Temp.**	**Press.**	**V-wind**	**U-wind**
Hub		0.012	0.031	0.014	0.009	0.007	0.012	0.003
Authority	0.028		0.037	0.013	0.009	0.031	0.001	0.018
FSI	0.033	0.042		0.014	0.003	0.002	0.001	0.000
Rainfall	0.009	0.015	0.006		0.009	0.015	0.012	0.016
Temp.	0.001	0.013	0.012	0.014		0.002	0.000	0.004
Press.	0.008	0.002	0.003	0.004	0.003		0.001	0.000
V-wind	0.006	0.006	0.003	0.004	0.002	0.017		0.021
U-wind	0.020	0.004	0.004	0.000	0.003	0.014	0.000	

Table A.1: Granger causality coefficients: the table reports the results of the Granger causality analysis for $p = 2$ lags. Causality direction is from column variables to row variables.

	Hub	Authority	FSI	Rainfall	Temp.	Press.	V-wind	U-wind
Hub		0.031	0.053	0.015	0.006	0.019	0.013	0.008
Authority	0.092		0.039	0.011	0.011	0.048	0.002	0.027
FSI	0.037	0.059		0.016	0.005	0.010	0.004	0.010
Rainfall	0.008	0.023	0.006		0.007	0.014	0.012	0.014
Temp.	0.004	0.014	0.016	0.014		0.010	0.004	0.003
Press.	0.005	0.013	0.012	0.009	0.003		0.002	0.000
V-wind	0.002	0.004	0.005	0.011	0.001	0.016		0.021
U-wind	0.020	0.009	0.013	0.000	0.008	0.011	0.001	

Table A.2: Granger causality coefficients: the table reports the results of the Granger causality analysis for $p = 3$ lags. Causality direction is from column variables to row variables.

	Hub	Authority	FSI	Rainfall	Temp.	Press.	V-wind	U-wind
Hub		0.060	0.083	0.025	0.010	0.051	0.038	0.024
Authority	0.104		0.051	0.018	0.014	0.052	0.015	0.032
FSI	0.066	0.105		0.050	0.019	0.009	0.007	0.019
Rainfall	0.014	0.027	0.008		0.027	0.012	0.028	0.013
Temp.	0.002	0.012	0.037	0.023		0.013	0.008	0.011
Press.	0.007	0.021	0.013	0.013	0.009		0.011	0.006
V-wind	0.021	0.001	0.016	0.022	0.004	0.029		0.035
U-wind	0.025	0.032	0.016	0.012	0.014	0.017	0.013	

Table A.3: Granger causality coefficients: the table reports the results of the Granger causality analysis for $p = 5$ lags. Causality direction is from column variables to row variables.